Physics at LEP-1 and LEP-2

by E. Fernández*

UAB/IFAE, Campus Univ. Autnoma de Barcelona, Edif. Cn
08193 Bellaterra, Barcelona, Spain
E-mail: enrique.fernandez@ifae.es

Abstract: Some of the physics being studied at the LEP-1 and LEP-2 accelerators is discussed. It includes precision electroweak measurements at the Z peak, fermion-pair production above the Z, WW cross-section measurements at LEP-2, the measurement of the W mass and its significance in the context of precision results, and Higgs boson searches.

1. Introduction

The LEP accelerator was inaugurated on 14th of July 1989 and has been delivering e^+e^- collisions since then, with an impressive performance. The four LEP experiments, ALEPH, DELPHI, L3 and OPAL, have each collected about 4.5 million events at energies near the Z resonance. From just before LEP, and until quite recently, the SLC Linear Collider at SLAC has also been working, delivering first a small luminosity to the Mark-II detector and then a substantial amount to the SLD, about 0.5 million events, with the unique feature of highly polarized electrons. The SLD has finally collected about 0.5 million events. From LEP and SLC, the Z properties, such as the mass, the total and partial widths and the couplings to fermions, have been measured with great precision. Since their values are sensitive to higher than first order radiative corrections, these measurements allow testing the electro-weak theory beyond tree level. The analysis of these data is nearly finished, and some of the results will not be improved for quite some time, since no other accelerator is foreseen at the moment at this energy region. This is explained in sections 2 and 12.

Since 1985, LEP has been running at center of mass energies well above the Z mass, reaching 208 GeV very recently. In this phase of LEP, LEP-2, the accelerator has also worked impressively and that has allowed the study of many topics, a few of which are covered in these lectures (sections 3 to 14).

It should be stressed that the whole body of knowledge accumulated by the study of LEP and SLD data is simply enormous. Many people, almost two thousand, have been working very hard for over 10 years, and this has translated into over 150 publications per experiment. It is clearly impossible to cover all the physics studied at LEP and SLC, not only in two lectures but in the whole week of the conference. I have chosen to cover the topics, at both LEP-1 and LEP-2, which are more related to electro-weak physics, and even within this topic, what is presented here is incomplete. In particular I say nothing about tau and b-physics at LEP-1/SLC and I do not cover in detail, for lack of time, the very recent measurements of the ZZ cross-section at LEP-2.

I hope nevertheless that these lectures are of some interest for the students here. For the LEP-1 and SLC literature I just refer to some recent reviews and to the very complete summary of the LEP and SLD Electroweak Working Group [3]. For LEP-2, I have tried to list of the original publications on the topics discussed, and I encourage the readers to directly consult them, whenever possible.

*Work supported in part by CICYT (AEN99-0837). These notes cover a part of the talks given by the author at the Silafae-III Symposium in Cartagena de Indias, Colombia, April 2-8, 2000.

2. Electroweak physics at LEP-1/SLC

The electro-weak measurements at LEP and SLC have been presented in practically all the major conferences in High Energy Physics for the last 10 years. For the latest reviews see [1,2]. The data presented here are those made available for the summer conferences of 1999. No significant changes have been presented since then [3].

2.1 Measurement of electro-weak observables

The program of electro-weak measurements at LEP goes as follows:

- The first step is to measure some *direct* observables, namely the *cross-sections* for the reactions

  $$e^+e^- \rightarrow \ e^+e^-, \mu^+\mu^-, \tau^+\tau^-, q\bar{q}$$

  as a function of the *beam energy* (the "lineshapes") and the forward-backward charge asymmetries (referred to as forward-backward asymmetries, for short) for those same processes, when possible, also as a function of the beam energy. The forward-backward charge asymmetry is the difference between the cross-sections in the forward and backward hemispheres for a given $f\bar{f}$ final state, normalized to the total cross-section for that state

  $$A_{FB}^f = \frac{\sigma_F - \sigma_B}{\sigma_F + \sigma_B}$$

  where F and B refer to the forward and backward hemispheres, respectively. An event is in the forward hemisphere if the angle of the fermion with respect to the incoming e^- (or the angle of the antifermion with respect to the incoming e^+) is less than 90 degrees. It has been measured for the lepton-pair production reactions and for $e^+e^- \rightarrow q\bar{q}$, where $q = s, c, b$.

  The beam energy is precisely measured in LEP-1 by the resonant depolarization method [4,72], with an error of $\Delta E \approx 2 - 3 MeV$ (after correcting for many effects, such as earth-tides, passage of trains, etc). This corresponds to a precision of better than 0.5 per mil. The measurement of the cross-section requires the knowledge of the luminosity, which in turn requires the calculation and measurement of the Bhabha cross-section at very small angles. An important development in the last two years was the reduction on the theoretical error in this quantity, which is now known with a precision of 0.6×10^{-3} [5]. The cross-sections are typically known at LEP with precisions of 0.5%.

- The second step is to obtain from the lineshapes, following the formulae explained in the next sections, the mass of the Z, its total width and its partial widths into leptons and hadrons. Obtaining the widths requires taking into account radiative corrections, which account for initial state-radiation (known to order α^3) and final state gluon radiation in the case of the hadrons (known to order α_s^3).

- In a third step other quantities are derived, namely R_e, R_μ and R_τ, where R_l is defined as the ratio of the Z partial width into lepton l divided by the partial width into hadrons.

From this procedure 9 quantities are obtained. At LEP these 9 quantities are calculated by each of the four experiments and the results are combined (by the "LEP electroweak working group") [3], taking into account common systematic errors. The results are given in Table 1. The upper index 0 refers to the value at the peak of the resonance.

It should be remarked that the precision of the above measurements is far superior to the most optimistic expectations before the start of LEP [6]. This is due to the progress on the understanding and calculations of the radiative corrections on the theoretical side, and to the great performance of the machine and detectors on the experimental side. The energy of LEP and its luminosity were measured with great precision and the cleaniness of the events and of their classification also exceeded the expectations. As an example, the lineshape into hadrons measured by the L3 collaboration and the forward-backward

m_z	91187.2 ± 2.1 MeV
Γ_z	2499.4 ± 2.4 MeV
σ^0_{had}	41.544 ± 0.037 nb
R_e	20.803 ± 0.049
R_μ	20.786 ± 0.033
R_τ	20.764 ± 0.045
$A^{0,e}_{FB}$	0.0145 ± 0.0024
$A^{0,\mu}_{FB}$	0.0167 ± 0.0013
$A^{0,\tau}_{FB}$	0.0188 ± 0.0017

Table 1: The basic LEP electro-weak observables, as of January 2000 [3].

asymmetry for muons measured by the ALEPH collaboration are shown in Fig. 1.

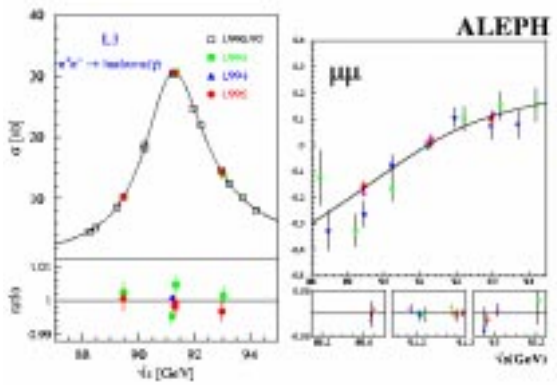

Figure 1: The lineshape for $e^+e^- \to q\bar{q}$ measured by L3 and the forward-backward asymmetry for $e^+e^- \to \mu^+\mu^-$ measured by ALEPH, both at LEP-1. The plots at the bottom show the difference between the measured values and the results of the fits to the theoretical expectations explained in sections 2.2-2.4.

In addition to the above, there are other observables which are also measured at LEP and SLC, namely the polarization asymmetries, defined below. They are related to the polarization of the final state fermions in the reaction $e^+e^- \to f\bar{f}$, and, in the case of the SLC, to the polarization of the incoming e^- beam.

In $e^+e^- \to f\bar{f}$, the fermions f and $\bar{f}$ are polarized (even if the incoming beams are not), that is, their spin points preferentially in one direction. Moreover, this polarization is correlated with the production angle. The polarization arises from the chiral nature of the weak current and from the approximate conservation of helicity at large energies. In practice the polarization can only be measured for the $\tau^+\tau^-$ final state, since the taus decay inside the detector and their spin can be inferred, statistically, from the angular properties of their decay products (this again follows from the properties of the weak charged current responsible for tau decay).

At LEP there are two quantities which are measured: the average longitudinal polarization, $\mathcal{P}_\tau$, and the forward-backward polarization asymmetry $A^{FB}_{\tau POL}$. These quantities are defined by

$$\mathcal{P}_\tau(s) = \frac{\sigma^{tot}_+(s) - \sigma^{tot}_-(s)}{\sigma^{tot}(s)}$$

$$A^{FB}_{\tau POL}(s) = \frac{(\sigma^F_+(s) - \sigma^F_-(s)) - (\sigma^B_+(s) - \sigma^B_-(s))}{\sigma^{tot}(s)}$$

where the $+$ and $-$ refer to the τ helicity, and the F and B refer to the forward and backward hemispheres, respectively.

At the SLC the electron beam can be polarized to a high degree (above 70% for most of the SLD data). Furthermore, the left and right (negative and positive helicity) luminosities are almost equal. This allows the measurement of other two quantities: the left-right polarization asymmetry and the left-right forward-backward polarization asymmetry (for each fermion f). They are measured at the peak energy and are given by

$$A^0_{LR} = \frac{1}{\mathcal{P}_e}\frac{\sigma_L - \sigma_R}{\sigma_L + \sigma_R}$$

$$\tilde{A}^f_{FB} = \frac{(\sigma^F_{Lf} - \sigma^B_{Lf}) - (\sigma^F_{Rf} - \sigma^B_{Rf})}{\sigma^{tot}}$$

where σ_L and σ_R are the total Z cross-sections for left (L) and right (R) electron polarizations, F and B refer to the forward and backward hemispheres, and the sub-index f stands for the Z cross-section into the corresponding $f\bar{f}$ final state. The quantity $\mathcal{P}_e$ is the polarization (luminosity-averaged) of the electron beam, which is measured in several ways with a relative error of 0.5% [2].

2.2 Interpreting the data within the Standard Model

As we will see in the following sections, the many

observables described above can be expressed within the Standard Model in terms of a few parameters. The measurements over-constrain the theory and thus can be used to test its consistency and to improve and/or constraint the values of the parameters.

From the line-shapes one obtains the widths and the mass of the Z, m_Z, with great precision. This is possible by fitting the line-shapes to a model-independent formula, which is just a modified Breigth-Wigner, as explained in section 2.4. In this fit, initial state photon radiation and final state gluon radiation, in the case of quark final states, have to be taken into account. In a further step, the widths, and the other observables described, can all be expressed in terms of the mass of the Z, m_Z, the Fermi constant, G_F, the electromagnetic coupling constant α, the strong coupling constant, α_s, the mass of the top, m^2_{top} (actually the difference of the squares of the masses of each of the quark doublets which, given the actual numerical dependence reduce to only m^2_{top}) and the logarithm of the Higgs mass, $log\ m_H$. The corresponding expressions come from the detailed calculation of higher order radiative corrections, carried out in detail over the past 15 years [7,8,9].

In section 2.3 we explain the first-order description of the observables, while section 2.4 briefly explains how to introduce the radiative corrections. In practice the data are fitted with the help of programs which incorporate the latest calculations of all known corrections [10,11]. In section 2.5 there are described some of the tests of the standard model, derived from the data. Only the main formulae and results are explained here. For a more detailed analysis see for example [12].

2.3 First-order description of the electroweak observables

The first order description of the $e^+e^- \rightarrow f\bar{f}$ process is given by the diagrams of Fig. 2.

The cross-section has three terms, corresponding to the exchange of the γ, the exchange of the Z, and the interference between them.

$$\sigma(s) = \sigma_\gamma(s) + \sigma_{\gamma Z}(s) + \sigma_Z(s)$$

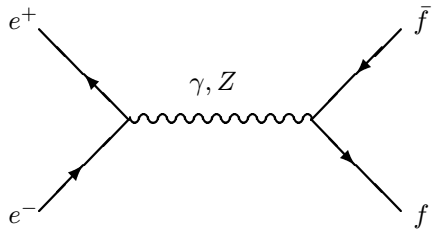

Figure 2: First order Feynman diagrams for $e^+e^- \rightarrow f\bar{f}$.

(For the $e^+e^- \rightarrow e^+e^-$ case there is the additional t-channel photon exchange diagram, which has to be added, or, alternatively, the data have to be corrected to "effectively remove" its contribution [3]. It is not considered any further here).

The γ annihilation diagram gives

$$\sigma_\gamma = \frac{4\pi\alpha^2}{3s}(N_f^c)^2 Q_f^2$$

where α is the fine structure constant, N_f^c is the color factor (1 for f=leptons, 3 for f=quarks), and Q_f is the electric charge of the final state fermion. The interference term is very small at the peak and can be included as a correction, calculated in the SM. The term due to the resonant Z exchange can be parameterized, in a model independent way, as a function of the total width of the Z, Γ_Z, and the partial widths Γ_e, Γ_f, of the Z into electron (arising from the production) and f pairs (arising from the decay), respectively,

$$\sigma_Z^{f\bar{f}}(s) = \frac{12\pi}{m_Z^2}\frac{\Gamma_e\Gamma_f}{\Gamma_z}\frac{s\Gamma_Z^2}{(s-m_Z^2)^2 + m_Z^2\Gamma_Z^2}$$

This formula reflects the resonant nature of the cross-section when the center of mass energy is equal to the Z mass.

The widths depend on the coupling of the Z to fermions, which in the Standard Model involve two different constants: the vector and axial vector weak neutral current couplings which we will write as g_{Vf} and g_{Af}.

At tree level the widths are given by the following relations:

$$\Gamma_f = \frac{N_f^c G_F m_Z^3}{6\sqrt{2}\pi}(g_{Vf}^2 + g_{Af}^2)\ ;\quad \Gamma_Z = \sum_f \Gamma_f$$

where N_f^c is again the color factor, m_Z is the Z mass, G_F is the Fermi constant and g_{Vf} and g_{Af} are the vector and axial vector coupling constants. They are given in the S.M. in terms of the third component of the weak isospin for the corresponding fermion, I_3^f, and the electro-weak mixing angle $\sin^2\theta_W$:

$$\begin{aligned} g_{Vf} &= (I_3^f - 2Q_f \sin^2\theta_W) \\ g_{Af} &= I_3^f \end{aligned}$$

The forward-backward and polarization asymmetries can also be written in terms of the coupling constants. Their expression is particularly simple at the peak, $\sqrt{s} = m_Z$, where they are given by

$$\begin{aligned} A_{FB}^f &= \frac{3}{4} A_e A_f \\ \mathcal{P}_\tau(m_Z^2) &= -A_\tau \\ A_{\tau POL}^{FB}(m_Z^2) &= -\frac{3}{4} A_e \\ A_{LR}^0(m_Z^2) &= A_e \\ \tilde{A}_{FB}^f(m_Z^2) &= \frac{3}{4} \mathcal{P}_e A_f \end{aligned}$$

where A_f is given by

$$A_f = \frac{2 g_{Vf} g_{Af}}{g_{Vf}^2 + g_{Af}^2}$$

The quantities A_f are referred to as "polarization asymmetry parameters" or "asymmetry parameters", for short.

At tree-level

$$\begin{aligned} \sin^2\theta_W &= 1 - \frac{M_W^2}{m_Z^2} \\ G_F &= \frac{\pi\alpha}{\sqrt{2} M_W^2} \frac{1}{\sin^2\theta_W} \end{aligned}$$

where m_W is the mass of the W-boson and α is the electromagnetic coupling constant.

Notice that, because of the above relations, at tree level we could express any of the observables in terms of just 3 parameters, for example α, G_F and m_Z, that is,

$$O_i = O_i(\alpha, G_F, m_Z)$$

where O_i stands for any of the widths, asymmetries or ratios of widths.

2.4 Higher-order description of the electroweak observables

The special relevance of LEP comes from the fact that, with the level of precision at which the lineshapes (and hence the widths) and the other observables introduced in section 2.1 are measured, the tree-level relations are not adequate to describe the data, but it is necessary to introduce higher order radiative corrections. This has allowed to test the Standard Model beyond tree level, whith an impressive success, as it is explained below.

The radiative corrections can be divided into "photonic" (or pure QED) and "non-photonic" (electroweak) corrections. The most important photonic correction is that due to initial state radiation. It can be included by convoluting a radiator function (probability of radiating a certain energy from the initial state) with the cross-section at the corresponding reduced center of mass energy, $\hat{\sigma}$, which has the form of section 2.3, with suitable modifications to introduce the electroweak corrections (see below). Initial state radiation has the important effect of displacing the peak cross section by about $+90MeV$ from the Z mass and of lowering the cross section at the peak by about 30%.

Of the electroweak corrections the most important are those corresponding to vacuum polarization diagrams (they are also called "oblique corrections") They have a property called non-decoupling: masses much larger than those of the Z show up in the corrections and do not vanish. In particular the top and the Higgs masses give contributions proportional to the square of the mass, m_t^2, and to the logarithm of the Higss mass, $log\ m_H$, respectively.

There are several schemes to introduce the electroweak corrections. A particularly convenient scheme for LEP-1 is that of effective couplings: the radiatively corrected cross-section is written in terms of the widths as in tree level (with a modification consisting on replacing the width term in the denominator, $m_Z^2\Gamma_Z^2$, by a "s-dependent width", $(s\Gamma_Z/m_Z)^2$), and the widths are also given in terms of the coupling constants as in tree level, but the coupling constants now become "effective coupling constants"

$$\bar{\alpha}(s), \bar{\alpha_s}(s), \bar{g}_{Af}(s), \bar{g}_{Vf}(s)$$

These is usually referred to as the "improved Born approximation". Here the coupling constants are complex quantities which depend on the energy scale s ($s = m_Z^2$ at the Z peak) and on the fermion masses, in particular m_{top}^2, and on $log\ m_H$. The reader is referred to [12] for the explicit relations. In particular the calculated value of the electromagnetic coupling constant at $s = m_Z^2$ is

$$\alpha^{-1}(m_Z^2) = 128.89 \pm 0.09$$

while

$$\alpha^{-1}(0) = 137.0359895(61).$$

The uncertainty on $\alpha(m_Z^2)$ is dominated by non-perturbative effects on quark-loop contributions to the vacuum polarization corrections, which can however be supplemented by low-energy data on e^+e^- interactions. An analysis [14] parametrizes the uncertainty on α due to the 5 low mass quarks as

$$\Delta\alpha_{had}^{(5)} = 0.02804 \pm 0.00065.$$

This is the principal component of the error on $\alpha(m_Z^2)$ above. Unfortunately the low energy data do not allow a better accuracy. This uncertainty is presently limiting the precision of some of the electroweak tests mentioned in section 2.5.

The most relevant formulae are:

$$\begin{aligned}
\hat{\sigma}_Z^{f\bar{f}} &= \sigma_{f\bar{f}}^0 \frac{1}{1+\delta_{QED}} \frac{s\Gamma_Z^2}{(s-m_Z^2)^2 + (\frac{s\Gamma_Z}{m_Z})^2} \\
\sigma_{f\bar{f}}^0 &= \frac{12\pi}{m_Z^2} \frac{\Gamma_e \Gamma_f}{\Gamma_Z} \\
\bar{g}_{Vf} &= \sqrt{\rho^f}(I_3^f - 2Q_f \sin^2\theta_{eff}^f(m_Z^2)) \\
\bar{g}_{Af} &= \sqrt{\rho^f} I_3^f \\
\delta_{QED} &= \frac{3\alpha}{4\pi}
\end{aligned}$$

The ρ parameter is not equal to 1, as at tree level, but it is affected by the radiative corrections and depends in principle on the final state fermion f. The electroweak mixing angle is not related to m_W and m_Z as in tree level. It is also a function of the scale s and of the final state fermion f. The other formulae of section 2.3 are still valid, with the couplings replaced by effective couplings. In particular the asymmetry parameters A_f are given by

$$A_f = \frac{2\bar{g}_{Vf}\bar{g}_{Af}}{\bar{g}_{Vf}^2 + \bar{g}_{Af}^2}$$

As a consequence of the radiative corrections what we have now is that any observable O_i can be expressed as a function

$$O_i = O_i(\alpha(m_Z^2), G_F, m_Z, m_f, m_H, \alpha_s(m_Z^2))$$

where the mass of the fermions, m_f, the mass of the Higgs, m_H, and α_s enter because of radiative corrections. The O_i have been computed in the SM with enough accuracy to test the data in a meaninful way. Since there are more observables than unknown parameters, the data allow not only to calculate them, but to test the internal consistency of the theory. This is explained in the next section, and also in section 12.

2.5 Results and Tests of the Electroweak Theory

In this section the results of LEP and SLC are presented and a discussion is given of their significance. Unless otherwise stated the data come from reference [3] where the specific publications of the collaborations are listed.

2.5.1 The Z resonance parameters

The basic parameters measured by the LEP collaborations, after the proper averaging done by the LEP electroweak working group, have already been presented in Table 1. Assuming lepton universality one obtains the averages R_l and $A_{FB}^{0,l}$ given in Table 2. Also on this table are given the widths into leptons, hadrons and "invisible particles" ($\Gamma_{inv} = \Gamma_Z - \Gamma_{ee} - \Gamma_{\mu\mu} - \Gamma_{\tau\tau} - \Gamma_h$) obtained from the fits to the lineshapes assuming lepton universality and the widths into electrons, muons and taus obtained without this assumption. Notice that the results are indeed compatiple with the hypothesis of lepton universality.

The Z mass, the Z total width, R_l and σ_{had}^0 are shown in Fig 3 for the four LEP experiments. The precision of the Z mass is limited by the LEP energy scale uncertainty, which contributes with a common 1.7 MeV systematic error to all

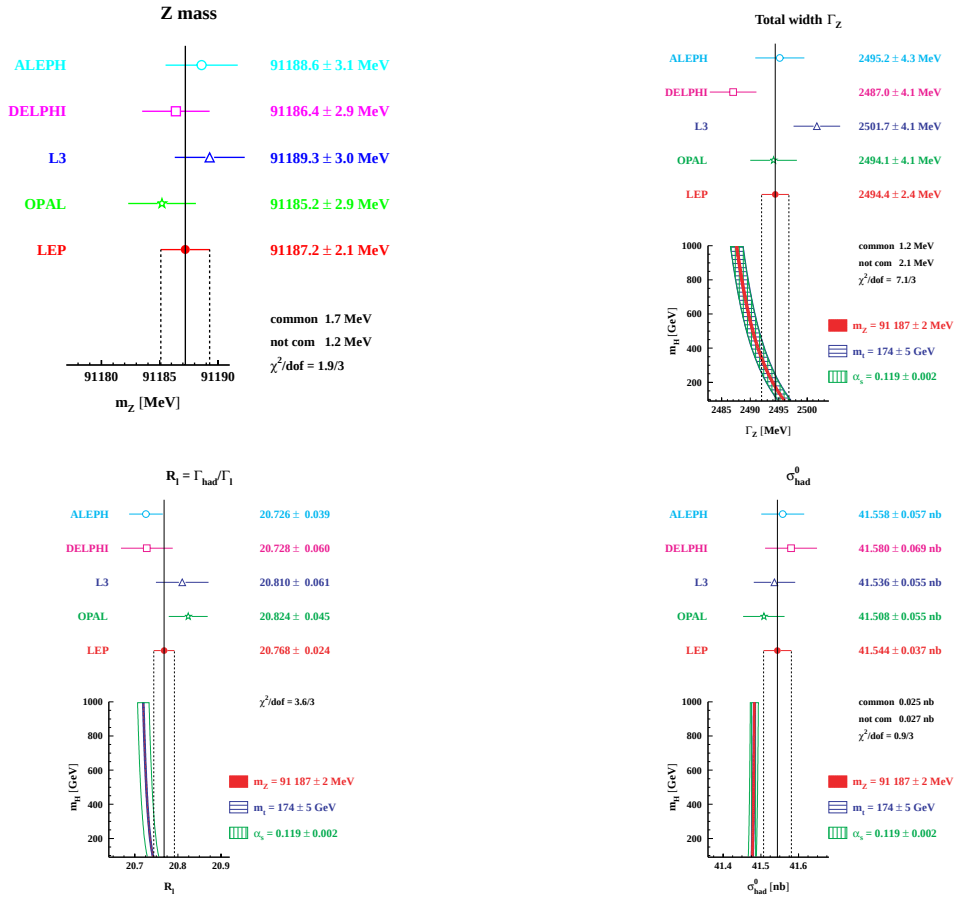

Figure 3: The Z mass, the Z width, the ratio of the hadronic to the leptonic widths (assuming lepton universality, and the hadronic peak cross-section from the LEP experiments. The sensitivity to the Higgs mass is shown as described in the text.

	With Lepton Universality
R_l	20.768 ± 0.024
$A_{FB}^{0,l}$	0.01701 ± 0.00095
Γ_{had}	1743.9 ± 2.0 MeV
Γ_l	83.959 ± 0.089 MeV
Γ_{inv}	498.80 ± 1.5 MeV
	Without Lepton Universality
Γ_{ee}	83.90 ± 0.12 MeV
$\Gamma_{\mu\mu}$	83.96 ± 0.18 MeV
$\Gamma_{\tau\tau}$	84.05 ± 0.22 MeV

Table 2: Electroweak observables with and without the assumption of lepton universality.

the measurements. The plot at the bottom of the measurements shows the dependence of the corresponding quantity on the Higgs mass. The bands correspond to 1σ variations of the top mass and of α_s as they are presently known. Notice that Γ_Z has a strong dependence on the Higgs mass while R_l and σ^0_{had} do not. This is due to the cancellation of the radiative corrections in these quantities, which are ratios of widths. From the plot it is clear that the measurement of Γ_Z does favor a low Higgs mass, a trend which is consistently present in the measurements of almost all of the electroweak observables.

Fig 4 shows the 68% confidence regions of the $A_{FB}^{0,l} - R_l$ plane, for the three leptons separately and assuming lepton universality (see fig. caption). Again, a low value of the Higgs mass is preferred by the measurements.

2.5.2 The number of neutrino species

An interesting derived quantity is the "invisible

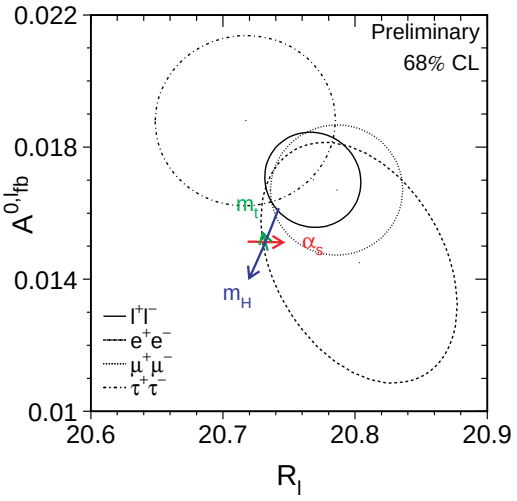

Figure 4: 68% confidence region in the $A^{0,l}_{FB} - R_l$ plane, for the three leptons separately and assuming lepton universality (solid line). The SM predictions for $m_Z = 91.1871$ GeV, $m_t = 174.3 \pm 5.1$ GeV, $m_H = 300^{+700}_{-205}$ GeV, and $\alpha_s(m_Z^2) = 0.119 \pm 0.002$ are also shown The intersection of the arrows correspond to the central values, and the arrows point in the direction of *increasing* values of m_t, m_H, and α_s [3].

width". It is due to the decay of the Z into "invisible" particles. Assuming that they are SM neutrinos, the number of neutrino families can be simply computed as the ratio

$$N_\nu = \frac{(\Gamma_{inv}/\Gamma_l)_{measured}}{(\Gamma_\nu/\Gamma_l)_{SM}}$$

where the label SM means calculated in the Standard Model. The result is

$$N_\nu = 2.9835 \pm 0.0083$$

which is 2σ below $N_\nu = 3$. The change in this result with respect to previous years can be traced to the increase of σ^0_{had}, which changed as a consequence of the inclusion of newer calculations of radiative corrections.

2.5.3 Leptonic polarization asymmetry parameters

Owing to the small size of g_{Vl}/g_{Al}, the leptonic asymmetry parameters are very sensitive to the electroweak corrections. This is easy to see by parametrizing them in terms of $\sin^2\theta^l_{eff}$. Assuming lepton universality one writes

$$\sin^2\theta^{eff}_W = \sin^2\theta^l_{eff}$$

and thus

$$A_l = \frac{2(1-4\sin^2\theta^{eff}_W)}{1+(1-4\sin^2\theta^{eff}_W)^2}$$

Simple propagation of errors on this formula tells us that

$$\delta A_l \simeq -8\delta\sin^2\theta^{eff}_W$$

and therefore a small variation on $\sin^2\theta^{eff}_W$ translates into a large change on A_l.

The asymmetry parameters have been measured in a number of ways. The best measurement is that of A_e obtained by the SLD collaboration from the measurement of the polarization left-right asymmetry, and it is shown in Table 3 taken from reference [2].

Year	A^0_{LR}
1992	$0.100 \pm 0.044 \pm 0.004$
1993	$0.1656 \pm 0.0071 \pm 0.0028$
1994/5	$0.15116 \pm 0.00421 \pm 0.00111$
1996	$0.15703 \pm 0.00573 \pm 0.00111$
1997/8	$0.14904 \pm 0.00240 \pm 0.00097$
Total	0.15108 ± 0.00218
χ^2/dof	5.58/4 (23%)

Table 3: The measured values of A^0_{LR} from SLD[2].

Other measurements of the asymmetry parameters come from the measurement of the tau polarization and its forward-backward asymmetry in LEP. They give A_e and A_τ as it is clear from the formulae of section 2.3. The averages of the four LEP collaborations are

$$A_e = 0.1483 \pm 0.0051 \qquad A_\tau = 0.1425 \pm 0.0044.$$

The SLD collaboration also measures A_e, A_μ and A_τ from the left-right forward-backward asymmetries $\tilde{A}^f_{FB}$ in their leptonic channels. The results are [1,2]

$$A_e = 0.1558 \pm 0.0064$$

$$A_\mu = 0.137 \pm 0.016$$
$$A_\tau = 0.142 \pm 0.016$$

These measurements are again consistent with lepton universality and can be combined to give

$$A_l = 0.1523 \pm 0.0057$$

2.5.4 Leptonic coupling constants and lepton universality

The measurements of the widths, forward-backward asymmetries and asymmetry parameters for leptons can be casted in terms of the neutral current coupling constants g_V and g_A. This has been done in [3] and the results, including LEP and SLD data, are given in Table 4

	Without Lepton Universality
g_{Ve}	-0.03809 ± 0.00047
$g_{V\mu}$	-0.0360 ± 0.0024
$g_{V\tau}$	-0.0364 ± 0.0010
g_{Ae}	-0.50105 ± 0.00036
$g_{A\mu}$	-0.50117 ± 0.00054
$g_{A\tau}$	-0.50198 ± 0.00064
	Ratios of couplings
$g_{V\mu}/g_{Ve}$	0.946 ± 0.065
$g_{V\tau}/g_{Ve}$	0.955 ± 0.030
$g_{A\mu}/g_{Ae}$	1.0002 ± 0.0013
$g_{A\tau}/g_{Ae}$	1.0019 ± 0.0015
	With Lepton Universality
g_{Vl}	-0.03772 ± 0.00041
g_{Al}	-0.50117 ± 0.00027

Table 4: The neutral current couplings from LEP and SLC.

The ratios of the couplings, also shown in Table 4, test lepton universality with great accuracy (for the axial couplings the accuracy is similar to that of charged currents, tested in tau decay [13]).

The coupling to the neutral leptons, the neutrinos, can be derived from Γ_{inv} assuming "neutrino universality", $g_{A\nu} \equiv g_{V\nu} \equiv g_\nu$, and $\Gamma_{inv} = 3\Gamma_{\nu\nu}$. The result is [3] $g_\nu = +0.50058 \pm 0.00075$, where the sign has to be taken from neutrino scattering data (since the width only depends quadratically on the couplings).

Shown in Fig. 5, are the contour 68% confidence regions in the $g_V - g_A$ plane (see fig. 5 caption).

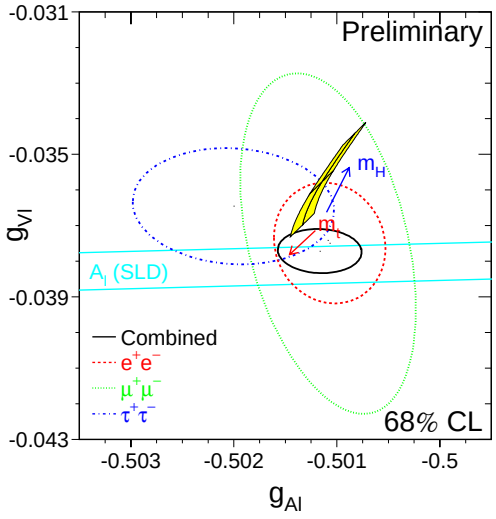

Figure 5: 68% confidence region in the $g_{Vl} - g_{Al}$ plane, allowed by the data of LEP and SLD. The dotted lines are for the individual lepton species and the solid line is the result assuming lepton universality. The SM allowed region for $m_Z = 91.1871$ GeV, $m_t = 174.3 \pm 5.1$ GeV, $m_H = 300^{+700}_{-205}$ GeV, and $\alpha_s(m_Z^2) = 0.119 \pm 0.002$ is also shown as the banana-shaped region. The arrows pont in the direction of *increasing* values of m_t, m_H, and α_s [3].

2.5.5 Quark asymmetries and Z-quark coupling constants

During the last three years there has been a lot of progress in measuring the Z to quarks couplings. The information comes from the measurement of several observables, namely R_b and R_c, measured at LEP and SLC (R_q is defined as the ratio $\Gamma_{q\bar{q}}/\Gamma_{had}$), the quark F-B asymmetries $A_{FB}^{0,b}$ and $A_{FB}^{0,c}$ measured at LEP, and the quark polarization asymmetry parameters A_b, A_c and A_s directly measured at the SLD from the left-right forward-backward asymmetry for events tagged as Z decaying into the corresponding $q\bar{q}$ final state. The polarization asymmetry parameters can also be obtained indirectly from the LEP data, by combining charged forward-backward (unpolarized) quark asymmetries and the mea-

surement of A_e obtained from the leptonic data (see equations of section 2.3).

R_b and R_c are measured at LEP and SLC by a variety of techniques (see [3] and references therein. The latest values are (see compilation in [2])

$$R_b = 0.21642 \pm 0.00073 \quad R_c = 0.1674 \pm 0.0038$$

which agree well with the SM values (for $m_t = 174.3 \pm 5.1$ GeV, $m_H = 100$ GeV)

$$R_b = 0.21579 \pm 0.000183 \quad R_c = 0.17228 \pm 0.00006$$

The average values of the forward-backward asymmetry and of the polarization asymmetry parameters for b and c quarks, from LEP and SLD, respectively, are given in Table. 5 [1,2]. A_s has also been measured directly by SLD and indirectly (combining the forward-backward asymmetry and A_e), by DELPHI and OPAL [2].

A^0_{FB}, b (LEP)	0.0988 ± 0.0020
A^0_{FB}, c (LEP)	0.0692 ± 0.0037
A_b (SLD)	0.905 ± 0.026
A_c (SLD)	0.634 ± 0.027

Table 5: The forward-backward (unpolarized) asymmetries for b and c quarks from LEP and the polarization asymmetry parameters A_b and A_c from the SLC.

The data agree with the standard Model predictions at the 1σ level. However, when they are combined among themselves and with the best value of A_l (needed to unfold A_b and A_c from $A^{0,b}_{FB}$ and $A^{0,c}_{FB}$) one obtains the results of Table. 6 [1]. The discrepancies of A_b and A_c from their SM values are of 2.7σ and 2.0σ, respectively. These discrepancies are likely to remain for some years to come, as the analysis of the data is almost final.

Shown in Fig. 6 are the values of A_b and A_c versus A_l as determined from LEP and SLC data [3].

2.5.6 The electroweak mixing angle

One useful way of comparing the different asymmetry measurements is to show the values of the electroweak mixing angle derived from them. This is shown in Fig. 7 (in this figure $< Q_{FB} >$ refers to the overall hadronic forward-backward asymmetry).

	LEP and SLD	SM
A_l	0.1497 ± 0.0016	$0.1431^{+0.0054}_{-0.0057}$
A_b	0.892 ± 0.016	0.935
A_c	0.625 ± 0.021	0.668

Table 6: The polarization asymmetry parameters from a combination of LEP and SLC data, for leptons and for b and c quarks, together with the values expected from the SM.

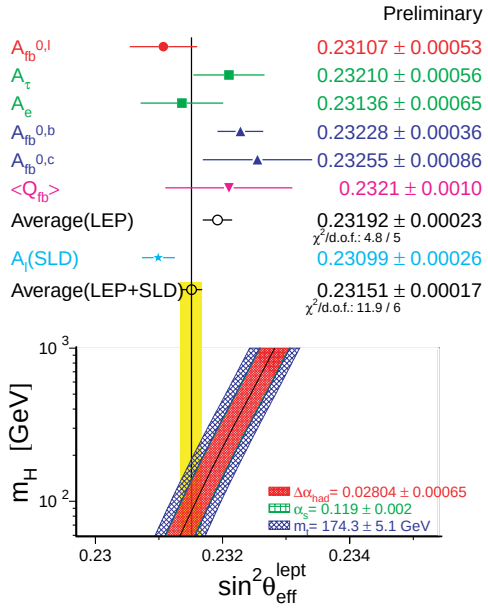

Figure 7: The values of $\sin^2\theta^{eff}_W$ extracted from several asymmetry measurements. The bottom plot is the SM prediction as a function of the Higgs mass. The bands correspond to the variation of m_t and the strong and electromagnetic coupling constants, as explained in the text [3].

The average of all measurements is

$$\sin^2\theta^{eff}_W = 0.23151 \pm 0.00017$$

In the figure it is also shown the prediction of the Standard Model as a function of the Higgs mass for $m_Z = 91.1871$, $1/\alpha(m^2_Z) = 128.878 \pm 0.090$ [14] and the indicated values of m_t and α_s. Again, a low value of the Higgs mass is indicated by the data.

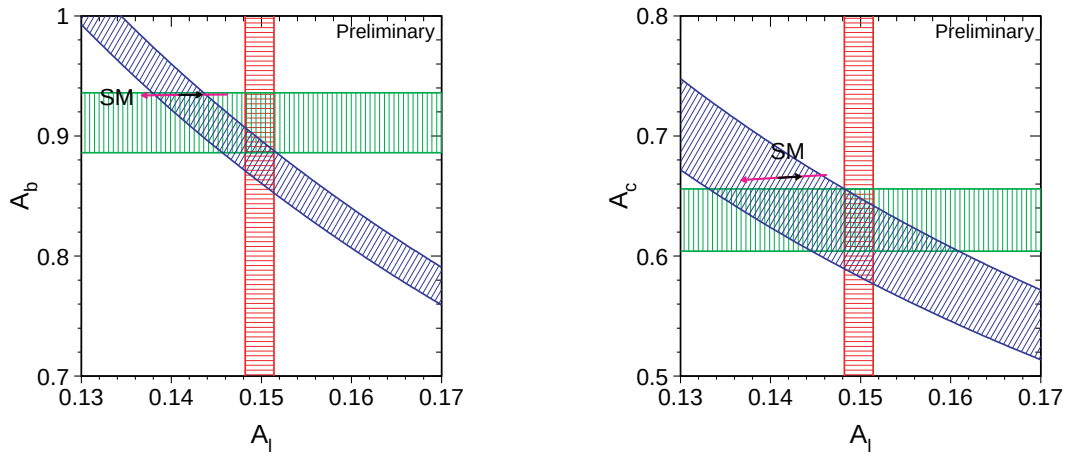

Figure 6: These two plots show the LEP and SLC combined measurement of the leptonic asymmetry parameter (vertical bands), the quark (b and c for the left and right figures, respectively) asymmetry parameter A_q from SLD (horizontal bands) and the forward-backward quark asymmetry $A_{FB}^{0,q}$ (diagonal bands). The left-pointing arrow shows the variation of the SM prediction for $m_H = 300^{+700}_{-205}$ GeV and the right-pointing arrow shows the SM prediction for $m_t = 174.3 \pm 5.1$ GeV [3].

On Fig. 8 the 68% confidence regions allowed by the data on the $sin^2\theta_W^{eff} - \Gamma_l$ plane (left side) and $m_t - m_H$ plane (right side) are shown. In both cases one sees again the preference for low Higg masses. The left figure also shows that the inclusion of electroweak non-photonic corrections is required to explain the data (see Fig. 8 caption). Further plots of this nature will be shown in section 12, after the explanation of the W mass measurements.

3. Running above the Z: LEP-2

LEP was planned, from the beginning, as a two-stage accelerator, with the aim of studying the Z resonance in a first phase and the reaction e^+e^-at higher energies, reaching the WW production threshold, in a second phase. This second phase, called LEP-2, was started in 1995, with short runs at center of mass energies of 130 to 136 GeV. The WW threshold (161 GeV) was reached in 1996 and since then the energy has been claiming steadily, having reached 208 GeV as of the time of this writing (July 2000).

Going above the Z the main first-order diagrams for the reaction are still those of Fig. 2, but the Z exchange is no longer resonant, and the total fermion-pair production cross-section follows the characteristic 1/s behavior. This can be seen in Fig. 9 for the specific channel $e^+e^- \to \mu^+\mu^-$. The fermion-pair production cross section above the peak will be studied in detail in the next sections. Other final states, and their respective cross-sections, are shown in Fig. 10. Notice in particular the sharp thresholds for WW and ZZ production. These reactions will also be studied in detail in future sections.

4. Fermion pair production at LEP-2

The cross-section for the production of $q\bar{q}$ pairs reaches about 41.5 nb (after corrections for initial state radiation) right at the Z peak. Well above this energy the cross-section is also dominated by fermion-pair production (with sharp thresholds for WW and ZZ production), but typical cross-sections are a factor of a thousand smaller than at the Z peak, thus resulting in much smaller

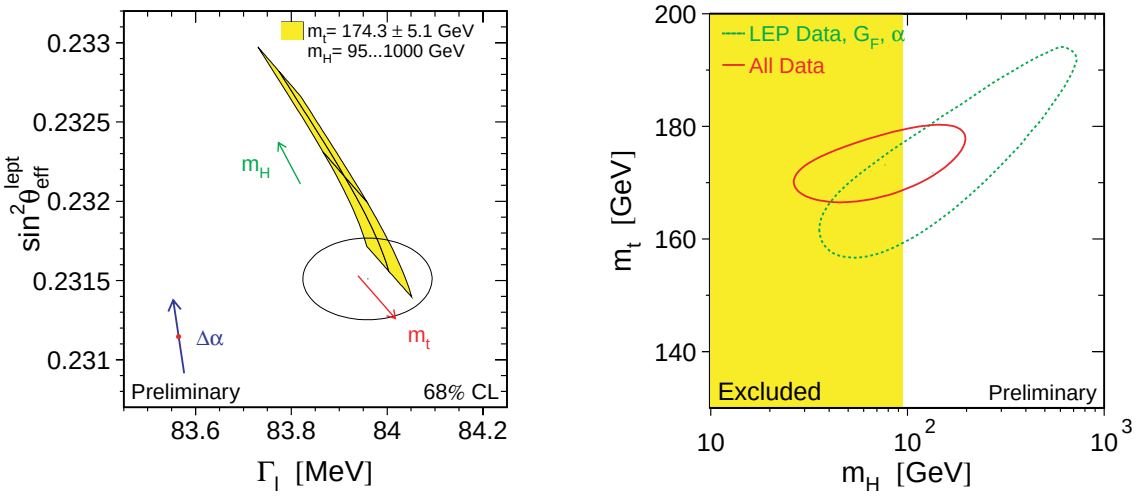

Figure 8: 68% confidence regions allowed by the data on the $sin^2\theta_W^{eff} - \Gamma_l$ plane (left side) and $m_t - m_H$ plane (right side). On the left side the shaded area is the SM prediction for the values of m_t and m_H indicated in the figure. The point with the arrow shows the SM prediction if only photon vacuum polarization corrections were included and the length of the arrow represents one standard deviation in the electromagnetic coupling constant α. To explain the measurements the electro-weak non-photonic corrections are clearly required. On the right plot the dotted line is what it is expected from LEP data alone, while the solid curve includes the direct CDF/D0 measurement of m_t [3].

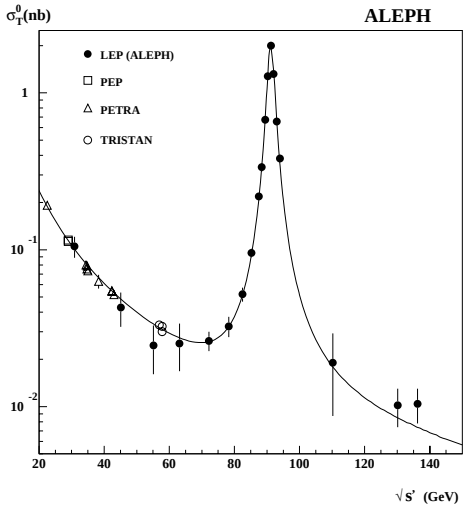

Figure 9: e^+e^- annihilation cross-section as a function of the collision energy, for the specific channel $e^+e^- \to \mu^+\mu^-$.

event samples than at LEP-1. This is shown in Fig. 10 [15]. To fix ideas: well above threshold the WW production cross-section is about 15 pb, that is, every inverse *pb* of accumulated luminosity gives 15 WW pairs. Shown in Table 7 are the energies and accumulated luminosities at which LEP-2 has operated. We are thus very far here from the huge data samples obtained at LEP-1.

Period	Energy (GeV)	Luminosity (pb^{-1})
1995	130/136	6.2
1996	161	12.1
1996	172	11.3
1997	183	63.8
1998	189	196.4
1999	192	30.

Table 7: Energies and integrated luminosities of LEP-2, up to July 1999.

Fermion-pair production has been extensively studied by the four LEP collaborations (see references [16] to [27]).

Initial state radiation has a dramatic effect at LEP-2. If, after radiation, the remaining center of mass energy of the e^+e^- pair is near the Z peak, the cross-section is highly enhanced (see below). Such events are called "radiative return events". Ideally we would like to separate them

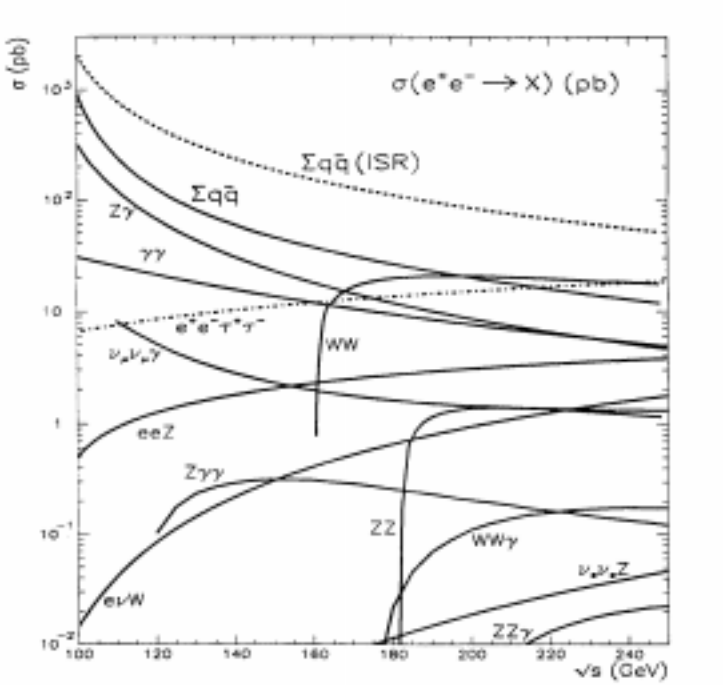

Figure 10: The e^+e^- annihilation cross-section at LEP-2 energies

from those with no radiation ("non-radiative"). For the latter the γ and Z exchange diagrams are of comparable importance.

The procedure to select radiative events involves finding photon(s) and jets of particles and, through kinematic fitting, test the consistency of initial state radiation. Once the photon(s) is removed, the center of mass energy after radiation, called s', can be computed from the four-momenta of the remaining particles. Thus two classes of events are defined:

(1) s'/s large (non-radiative)

(2) $s'/s > 0.01$ (inclusive)

where "large", in most analysis, means greater than 0.85. The s' distribution for $e^+e^- \to f\bar{f}$ at 183 GeV is shown in Fig. 11 for the OPAL experiment [26].

Two usual complications with this procedure are the following:

(a) Initial and final state radiation cannot be separated and, furthermore, they interfere. This makes difficult the definition of s'. Fortunately, the effect is small (1%) and can be "effectively removed" (calculated).

(b) Final states involving 4 fermions ($f_1\bar{f}_1f_2\bar{f}_2$), cannot be naturally separated from two fermion processes in some cases. This effect is taken into account when comparing the data with the theory.

All the LEP collaborations have studied these type of events and measured cross-sections and forward-backward charge asymmetries for $q\bar{q}$ and lepton-antilepton pair production. (See Figures 4 as an example of the measurement of the cross-section and leptonic forward-backward asymmetries).

Many topics have been studied from fermion pair production at high energies, some of which are summarized in the next subsections.

4.1 Comparisons with the Standard Model predictions

The results of the four LEP experiments are in very good agreement with the Standard Model predictions. A comparison of the latest data, from the four LEP experiments combined, with the SM expectations is shown in Fig. 13 [1,28].

Another comparison with the Standard Model was done by OPAL and is shown in Fig. 14 [26].

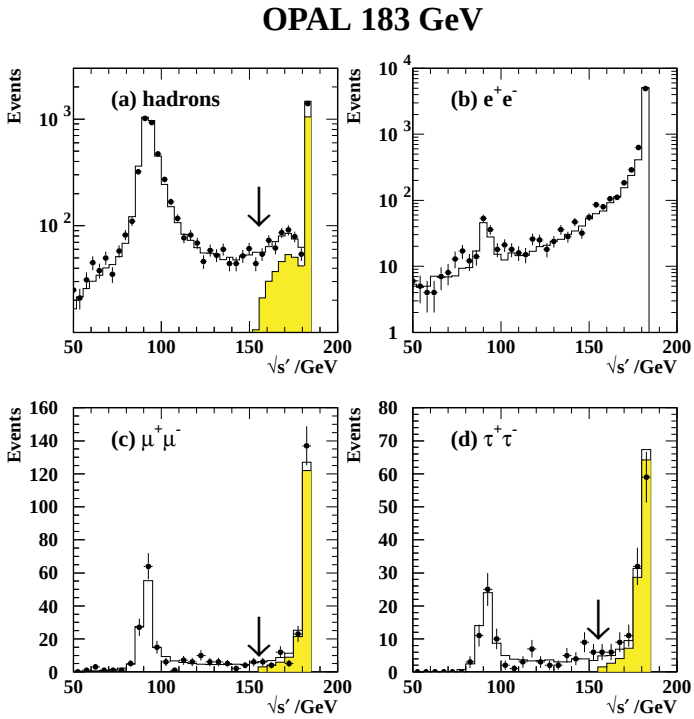

Figure 11: s-prime distribution for $e^+e^- \to f\bar{f}$ from OPAL [26].

Here the quantity R, defined as the ratio of the measured hadronic cross-section to the theoretical muon-pair cross-section is shown as a function of the center of mass-energy. The two sets of data points correspond to non-radiative events (open dots) and inclusive (all) hadronic events(black dots). The non-radiative cross-section (and the theoretical $\mu^+\mu^-$ cross-section) were corrected to Born level, where Born level means the improved Born approximation (see section 2.5) of the program ZFITTER, which was used to compute the corrections. In the inclusive data one can see the onset of WW and ZZ production, the latter very small and only at the point of 183 GeV energy. The dotted line at energies above 160 GeV is the prediction without WW (and ZZ) production, which is clearly required to explain the data. The figure also contains low energy data from PEP, PETRA and TRISTAN. At lower energies R is mainly $R\gamma$ (that is the cross section is dominated by the annihilation into a photon) and at the Z peak it is mainly R_Z. At the higher energies the γ and Z contributions are of similar importance.

Other interesting and more recent measurements are those related to b-quarks, made possible by the improved b-tagging capabilities of the LEP detectors. In particular R_b (see section 2.5.5) and the forward-backward charge asymmetry for b's, R^b_{FB}, have been measured up to the highest energies. The measurements at 189 GeV and their comparison with the SM are shown in Table 8[1,28]. The ALEPH measurements up to 183 GeV are shown in Fig. 15 [18].

	R_b	A^b_{FB}
ALEPH	0.151 ± 0.011	0.34 ± 0.19
DELPHI	0.167 ± 0.012	
L3	0.163 ± 0.016	0.66 ± 0.24
OPAL	0.167 ± 0.014	0.43 ± 0.17
LEP	0.161 ± 0.007	0.44 ± 0.12
SM	0.168	0.58

Table 8: The ratio of $b\bar{b}$ to $q\bar{q}$ production, R_b and the forward-backward asymmetry for $b\bar{b}$ final states at LEP-2 [1,28].

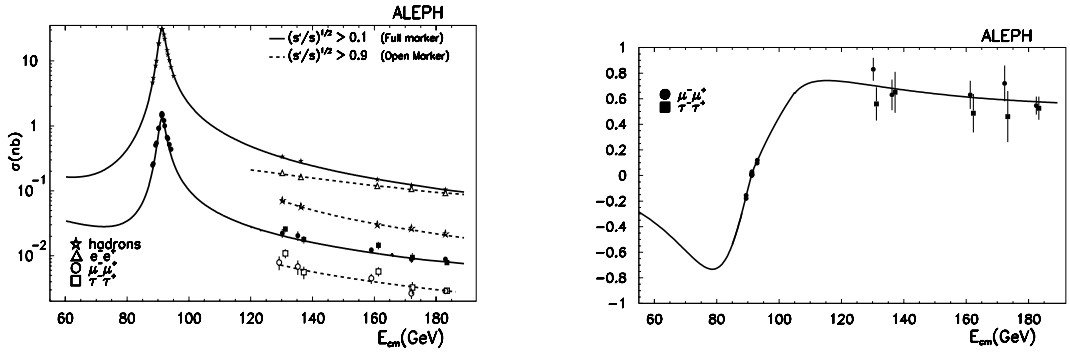

Figure 12: Measurements of the cross-sections for inclusive and non-radiative events and of the forward-backward leptonic (for μ and τ) asymmetries [18].

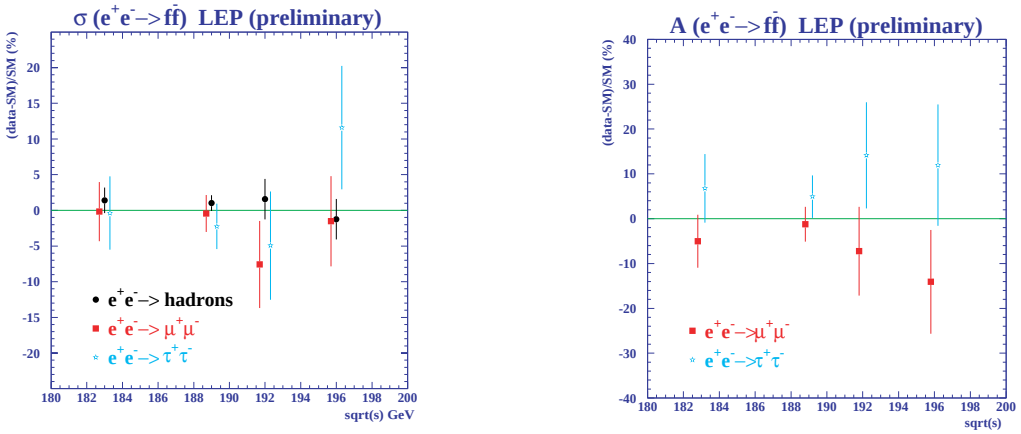

Figure 13: The e^+e^- annihilation cross-section and the leptonic forward-backward charge asymmetries for non-radiative events ($s'/s > 0.85$) minus the Standard Model expectation, for the four LEP experiments combined [1,28].

4.2 Measurement of the γ-Z interference

For non-radiative events the γ and Z diagrams have similar amplitudes and offer the opportunity of measuring the $\gamma - Z$ interference term (which was fixed to the SM value in the electroweak analysis at LEP1, as explained in section 2.3). Fig. 16 shows the OPAL determination of the quantity j^{tot}_{had}, which is a measure of the hadronic $Z-\gamma$ interference [25], versus the Z mass for events at the peak, and including LEP-2 data up to 172 GeV. The inclusion of the high-energy data considerably reduces the error with respect to LEP1 alone.

4.3 Measurement of the running of $\alpha(s)$

For non-radiative leptonic events the dominant diagram is γ exchange in the s channel. The corresponding cross-section is proportional to α^2. For hadronic events the dependence on α enters through both the photon exchange and the vector part of the Z exchange diagrams, but the effects tend to cancel.

OPAL has made a fit to the cross-sections for leptonic and hadronic final states, forward-backward asymmetries for muons and taus, and R_b [26].

Two analysis have been done:

(1) Fixing the other SM parameters (in ZFITTER). The result is

$$\alpha^{-1}(157.42\ GeV) = 119.2^{+5.1}_{-4.1}$$

The quoted $\sqrt{s}$ value is the luminosity-weighted average of the data sample. This result depends (through the luminosity) on the assumed running of α from Q^2=0 to typically $Q^2 = 3.5\ GeV^2$.

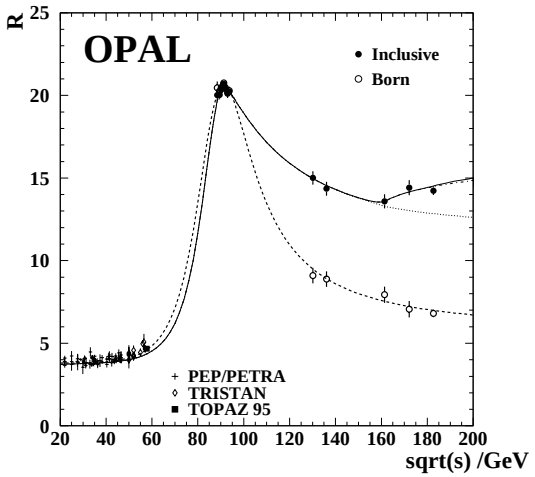

Figure 14: The ratio of the measured hadronic cross-section to the theoretical $\mu^+\mu^-$ cross-section. The open points correspond to the cross-section for non-radiative events, corrected to Born level, while the black points corresponds to inclusive events. The points at the peak and the theoretical $\mu^+\mu^-$ cross-section are also corrected to Born level (see text and ref. [26]).

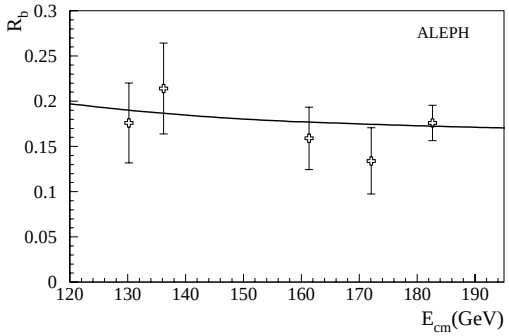

Figure 15: Aleph measurement of R_b up to 183 GeV energies, compared with the SM expectation[19]).

(2) Using measured values of $\sigma(\mu^+\mu^-)/\sigma(q\bar{q})$ and $\sigma(\tau^+\tau^-)/\sigma(q\bar{q})$. The result is

$$\alpha{-}1(157.42\ GeV) = 119.9^{+6.6}_{-5.4} \pm 0.1$$

which is independent of the running of at low Q^2. This value differs by 2.6 standard deviations from the value at $Q^2 = 0$. OPAL has also combined their measurements with those at TRISTAN. The result, extrapolated to the Z, is

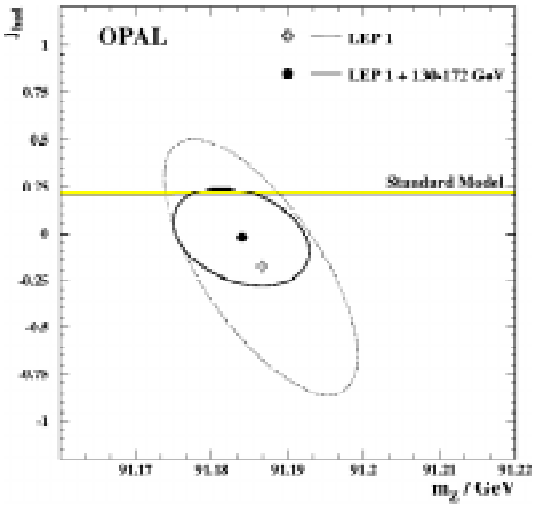

Figure 16: Measurement of the hadronic $\gamma - Z$ interference from OPAL [25].

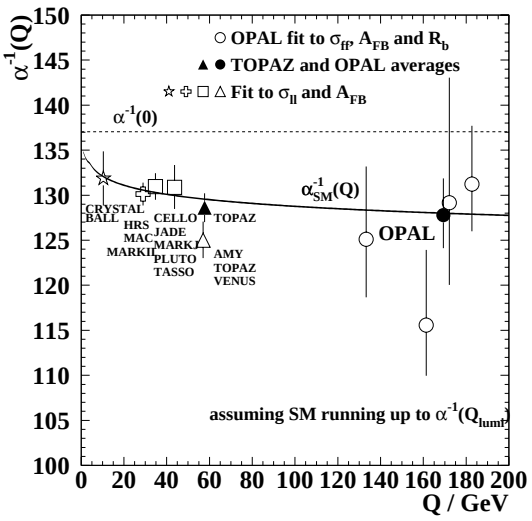

Figure 17: OPAL measurements of α_{em} together with measurements at lower energies [26].

$$\alpha^{-1}(m_Z) = 121.4^{+6.0}_{-4.9} \pm 0.1$$

(see Fig. 17). This result does not depend on assumptions about the running of α at low Q^2, which is the main uncertainty on the value of α_{em} used at LEP1 for electroweak analysis, as explained in sections 2.5.6. Unfortunately the result has a large statistical error.

4.4 Limits on four-fermion contact interactions

New interactions at a much higher energy-scale Λ, can show up at lower energies in extra terms in the SM Lagrangian

$$L = \frac{g^2}{(1+\delta)\Lambda^2} \sum_{i,j=L,R} \eta_{ij} [\bar{e}_i \gamma^\mu e_i][\bar{f}_j \gamma_\mu f_j]$$

where $e_{L,R}$ and $f_{L,R}$ are the left- and right-handed spinor projections, η_{ij} depend on the model and Λ is the energy scale of the new interaction. Λ can arise from the exchange of a very heavy particle, or can be due to substructure of the fermions, or, in a general way, can be considered as a parameterization of new physics.

The consequence of these terms is a dependence of the differential cross-section on:

$$\epsilon = \frac{g^2}{(1+\delta)\Lambda^2}$$

$$\frac{d\sigma}{d\cos\theta} = \sigma_{SM}(s,t) + C_2^0(s,t)\epsilon + C_4^0(s,t)\epsilon^2$$

where the C depends on the specific form of the extra interaction term.

Several models have been assumed and fitted to the data (after corrections, including e-w radiative corrections). The lower limits on their value, from OPAL [26], are shown in Fig. 18.

4.5 Limits on extra Z bosons

Extra Z bosons are present in many GUT theories, such as E6 (several varieties) and L-R models $(SUc(3) \bigotimes SUL(2) \bigotimes SUR(2) \bigotimes U_Y(1)$. A sequential Z' (same couplings as Z but higher mass) can also be present in a simple extension of the SM. For the latter, an ALEPH analysis [18] gives for example:

$$m'_Z(sequential) > 898\ GeV\ (at\ 95\%)$$

an less restrictive limits within several model scenarios.

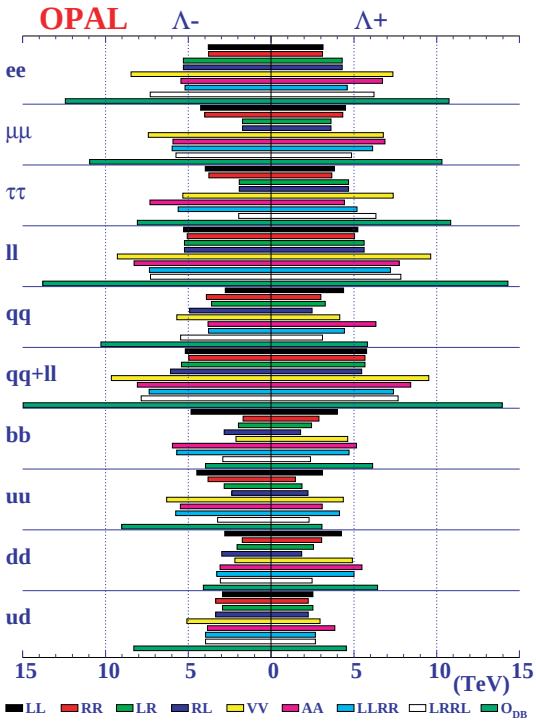

Figure 18: 95 % confidence limits of the energy scale from contact interactions. The bars for each channel correspond to different models, indicated at the bottom.

5. Single γ production and the number of neutrino families

Long before the start of LEP, the original though to measure the number of neutrino families contemplated running a few GeV above the Z peak and studying the cross section of the reaction $e^+e^- \rightarrow \nu\bar{\nu}\gamma$, where the γ comes from initial state radiation [29] (see Fig. 19). If the remaining center of mass energy after radiation of the γ is near the Z the cross-section is enhanced (again radiative return). Thus the energy of the radiative foton for the observed single gamma event coming from this reaction will have a peak, at an energy roughly equal to $\sqrt{s} - m_Z$, reflecting the Z peak. The size of the cross-section depends linearly on the number of neutrino families [30].

The experiment has been done by all the LEP collaborations giving $N_\nu = 3.00 \pm 0.08$ [31]. It has also been done at energies way above the Z mass. Data at $\sqrt{s} = 189$ GeV were presented

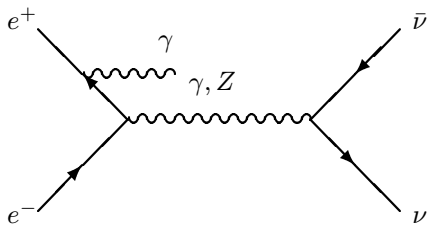

Figure 19: The single γ reaction lowest order diagram.

at the EPS-HEP-99 conference [1].

The cross section for single gamma agrees with the standard model expectation for 3 neutrino families. The average of the cross-section of the four LEP experiments gives $\sigma^{measured}/\sigma^{SM} = 0.965 \pm 0.028$. To extract the number of neutrinos one has to compare with a MC with specific cuts on the angle and energy of the photon. The average number of neutrino derived from these data is [1]

$$N_\nu = 2.99 \pm 0.10$$

which is similar in precision to that derived from the same method at energies just above the Z mentioned above, but much less precise than that derived from the width and cross-section at the peak of the Z mentioned in section 2.5.2.

The L3 single-gamma spectrum at $\sqrt{s} = 189$ GeV is shown as an example in Fig. 20) (left side) and the comparison of the cross-section for the single-gamma reaction at several LEP-2 energies (for $E_\gamma > 5$ GeV and polar angles such that $\cos\theta_\gamma \leq 0.97$) is shown on the same figure (right side).

6. Measurement of the WW production cross-section

One of the main goals of LEP-2 is the study of the reaction

$$e^+e^- \to W^+W^-$$

and in particular the measurement of its cross-section. This reaction involves the triple gauge boson vertices $Z - W - W$ and $\gamma - W - W$ predicted by the electroweak theory, which were never directly observed before LEP-2. All the LEP collaborations have studied the reaction extensively (see refs. [33] to [42]).

The measurement of the cross-section for WW production requires to select WW final states where the W's are "real" (resonant). There are 3 main diagrams (called CC03, Fig. 21) which contribute to this reaction:
Once produced, each W decays to two fermions, leading to a 4-fermion final state.

However, for any specific 4-fermion final state, there are many other ways in which it can be produced, which do not involve the above 3 diagrams. For example, for the specific channel $e^+e^- \to u\bar{d}\mu^-\nu_\mu$ (and $e^+e^- \to \bar{u}d\mu^+\bar{\nu_\mu}$) final state, there are 10 diagrams (see Fig. 22):

Therefore one has to agree on the meaning of "signal events". There is some flexibility on the exact criteria in that at the end one compares a selected sample of events with a "theory", presumably built up with the same criteria. In particular one could have a sample of events that includes four-fermion final states which do not come from resonant W's, provided the corresponding diagrams were included in the comparison with the theory.

The LEP collaborations follow slightly different procedures in treating the data, but in essence all methods consist on selecting events that mainly "come" from those diagrams (that is, an enriched sample of WW events), compute the theoretical "effective cross-section" for them, and then make the comparison. The effect of the other diagrams is corrected for, via MC simulation. For example, in ALEPH:

$$\sigma_{cc03} = \frac{N_{obs} - N_{back} - N_{4f}^{cc\bar{0}3}}{L\epsilon_{cc03}}$$

$$N_{4f}^{cc\bar{0}3} = L[\epsilon_{4f}^{MC} - \epsilon_{cc03}\sigma_{cc03}^{MC}]$$

where

N_{obs} = number of observed events, after cuts

N_{back} = number of events from non-like WW diagrams

$N_{4f}^{cc\bar{0}3}$ = number of events attributed to 4f, non-CC03 diagrams,

$\epsilon's =$ selection efficiencies (computed from MC).

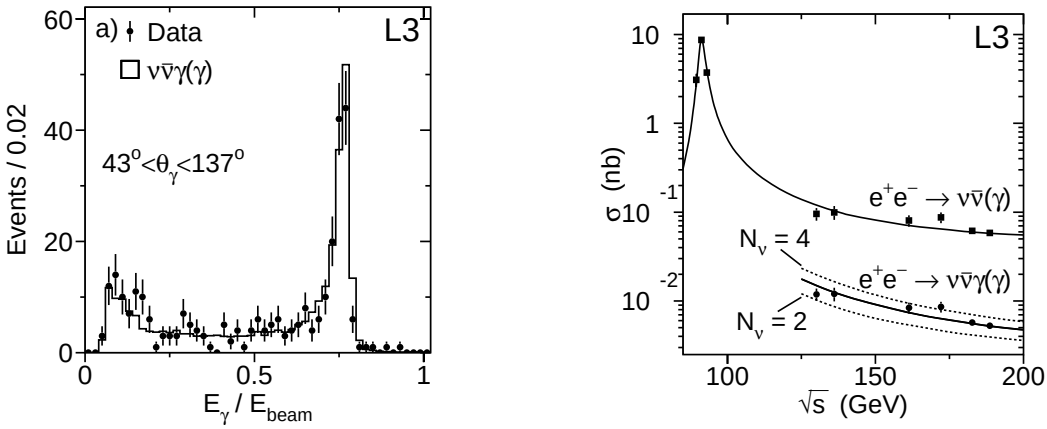

Figure 20: Single γ spectrum at $\sqrt{s} = 189$ GeV from L3 compared with MC expectations (left side) and $e^+e^- \rightarrow \ \nu\bar{\nu}\gamma$ cross-section (for $E_\gamma > 5$ GeV and $\cos\theta_\gamma \leq 0.97$) compared for the expectation for 2,3 and 4 neutrino families. The upper curve is the extrapolated full $e^+e^- \rightarrow \ \nu\bar{\nu}$ cross-section from peak energies to $\sqrt{s} = 189GeV$ [32].

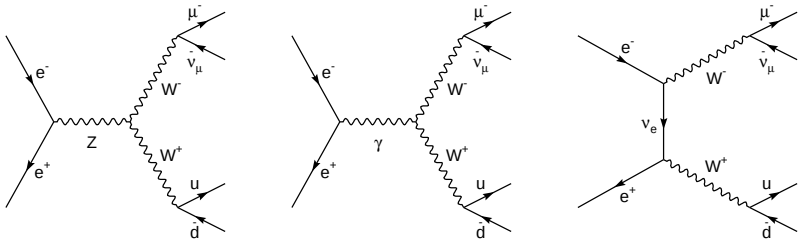

Figure 21: The CC03 diagrams for WW production in e^+e^- interactions.

The "4f-CC03 correction", $N_{4f}^{cc\bar{0}3}/L$, amounts to about 1% at most.

The W's decay leptonically ($l\nu$) or hadronically ($q_1\bar{q}_2$) and thus the events can be classified as:

(A) Fully leptonic:$e^+e^- \rightarrow l^+l^-\nu\bar{\nu}$,

(B) Semileptonic: $e^+e^- \rightarrow l\nu q_1\bar{q}_2$,

(C) Hadronic: $e^+e^- \rightarrow q_1\bar{q}_2q_3\bar{q}_4$.

The selection methods are different for each case, and so are the backgrounds. In general, the procedure to select these events consists on the following steps:

- Make loose cuts to get an "enriched" sample of WW events, and eliminate as much background as possible.
- Make a more refined selection to get N_{obs} for each of the final state classes considered (inclusive or exclusive).
- Apply $4f - C\bar{C}03$ correction to get cross sections.

The main background comes from

- $Z(\gamma)Z$ where $Z \rightarrow l^+l^-$ or $Z \rightarrow q\bar{q}$.
- $Z(gluon)$ where $Z \rightarrow l^+l^-$ or $Z \rightarrow q\bar{q}$.
- ZZ (above ZZ threshold), where $Z \rightarrow l^+l^-$ or $Z \rightarrow q\bar{q}$.

Radiative Z events have either a hard photon or missing momentum along the beam direction, hence the cuts on these characteristics.

All the LEP collaborations have developed sophisticated methods of selection for each of the different channels involved.

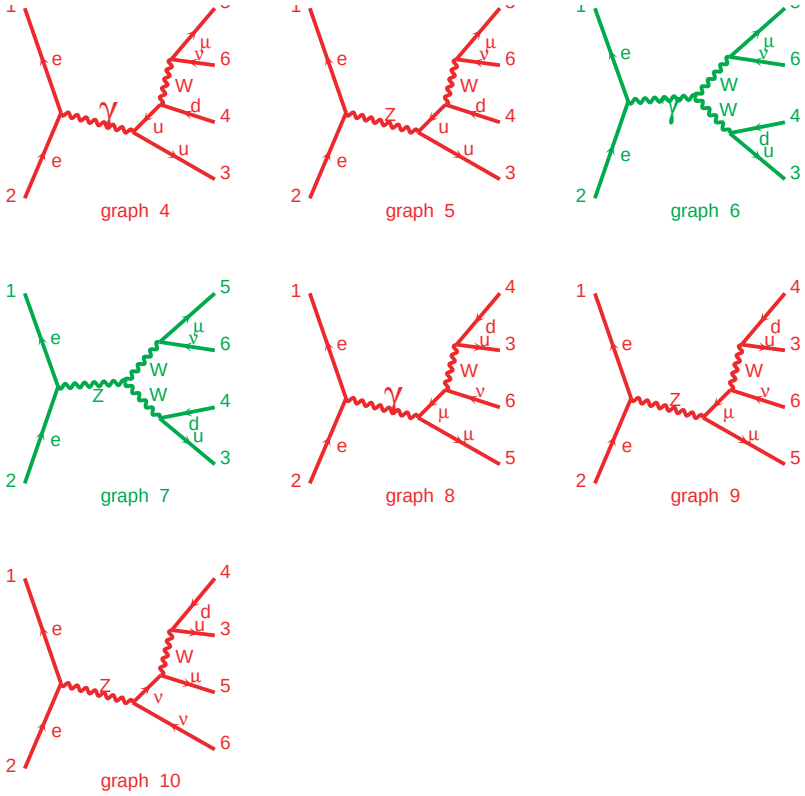

Figure 22: Diagrams contributing to the final state $e^+e^- \to ud\mu\nu_\mu$.

6.1 Selection of fully leptonic W decays ($e^+e^- \to l^+l^-\nu\bar{\nu}$)

These events are characterized by

- two energetic and acoplanar leptons of opposite charge,
- missing momentum due to the undetected neutrinos,
- if one lepton is a tau, a narrow jet in some cases.

giving rise to 3 types of events: (i) lepton-lepton, (ii) lepton-jet, (iii) jet-jet.

The events are selected by making appropriate cuts based on the above characteristics. Examples of the variables used are shown in Fig. 23 which displays the acoplanarity distribution of the two leptons in ALEPH (left) and the energy distribution of the leptons in L3(right). The arrows show the position of the cuts.

6.2 Selection of semi-leptonics decays ($e^+e^- \to l\nu q_1\bar{q}_2$)

These events typically have

- one lepton of energy > 40 GeV,
- large missing momentum,

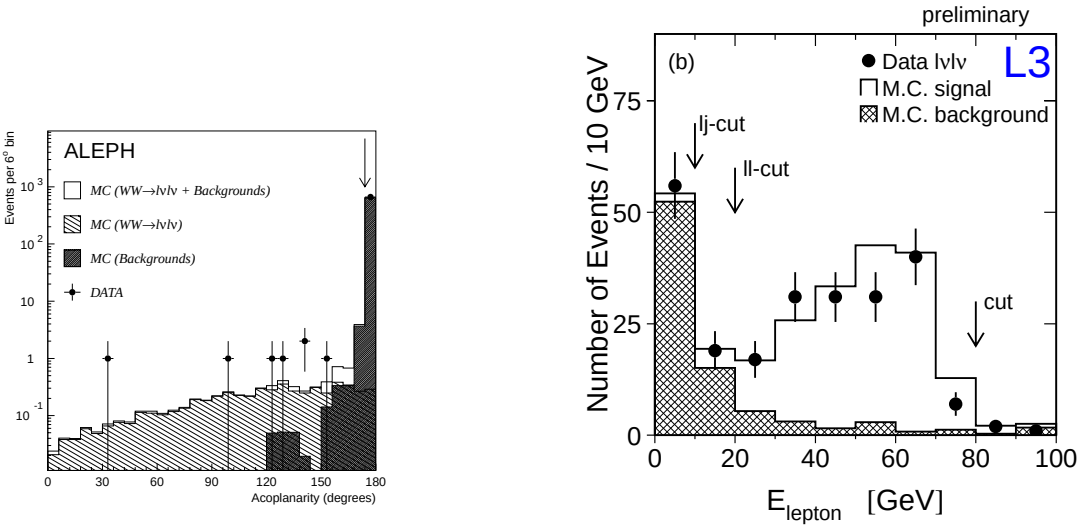

Figure 23: Acoplanarity angle of the two charged leptons (ALEPH) and lepton energy (L3) in purely leptonic decays of the $W's$.

- two hadronic jets, each of energy > 40 GeV.

An example of this kind of event, from ALEPH, is shown in Fig. 24.

The selection criteria for $l\nu q_1, \bar{q}_2$ are different for $l = e, \mu$ or $l = \tau$. For example in ALEPH the selection of $l\nu q_1\bar{q}_2 (l = e, \mu)$ events starts with a preselection which consists on finding the direction of the missing transverse momentum and taking as the lepton candidate the particle with the highest momentum antiparallel to the missing momentum. It is then required that the particle has momentum greater than 15GeV/c and that it is identified as an electron or a muon. After the preselection, three quantities, lepton energy, missing momentum and isolation angle, are examined, and a probability is then calculated, based on probability density functions for those quantities, obtained from a Monte Carlo sample of these type of events. A cut is then made on the event probability computed in this way, and the event is selected or rejected. The distributions of lepton energy, missing transverse momentum and isolation are shown in Fig. 24 for ALEPH. The probability distribution functions are shown in Figs. 25.

For the $\tau\nu q_1\bar{q}_2$ events the criteria are different. A cut is first made on global properties of the event and an explicit attempt is made to identify the tau.

At the end one obtains the number of events selected in each channel and the estimation (from MC) of efficiencies, cross-channel missassignments and backgrounds [35] (see the table of Fig. 26).

6.3 Selection of fully hadronic decays ($e^+e^- \to q_1\bar{q}_2q_3\bar{q}_4$)

About half of the WW events decay in this way. They are characterized by 4 separated and energetic jets. The main background comes again from qq(γ), qq(g) and, above ZZ threshold, ZZ events decaying into 4 quarks (a practically irreducible background). An example of such an event is in Fig. 27.

Many methods have been developed to select this channel, combining all the available information (event shape variables, invariant masses, etc.) in an optimal way.

As an example of the great amount of work that went into selecting this channel, we briefly describe the four methods that were used by ALEPH to select WW hadronic events at the threshold of the WW production [33], All of them start with a pre-selection (large visible energy, small missing momentum, 4 jets and others) of efficiency $\sim 90\%$, followed by a method of estimating the number of events in each channel:

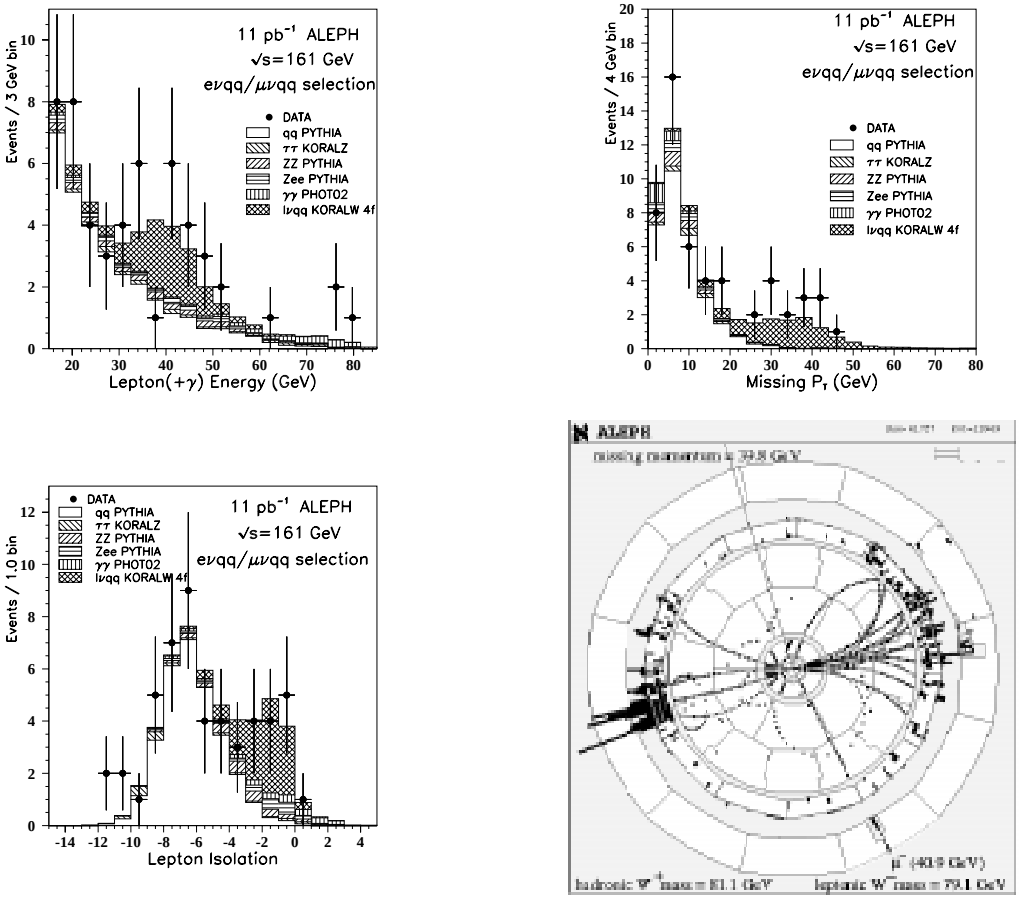

Figure 24: The distributions of lepton energy, transverse momentum and isolation variable for semileptonic WW events, as measured in the ALEPH detector. The bottom right figure is an example of such an event.

- Linear discriminant analysis :

$$U = \sum_i c_i x_i$$

  where x_i are variable which are different for signal and background (Durham y_{34}, minimum jet energy and others). Events are then selected by a cut in U.

- Rarity analysis : For each event a number of variables x_j are calculated, such that the value of x_j is small for background and large for signal. A new variable T_i, the fraction of MC WW events for which $x_j < x_j^i$ for all variables j, is computed. The Rarity R_i is the integral probability of T_i, that is the fraction of MC events for which $T < T_i$. This distribution is then fitted by a maximum likelihood method.

- Neural Network:a neural network incorporating 19 [35] or 14 [59] relevant variables (global event properties, jet properties, WW kinematics and others).

- Event weights: The cross sections are directly computed from the events, which enter with a weight, calculated by MC in a multi- dimensional space of discriminating variables.

These methods have been adapted for selection at higher energies. The results for the 4-jet channel are also shown in the Table of Fig. 26 [35].

Once the number of events in each channel are known, together with the expected background and efficiency matrix, the cross section can be calculated, e.g., by means of another max-likelihood fit: the cross sections for all the chan-

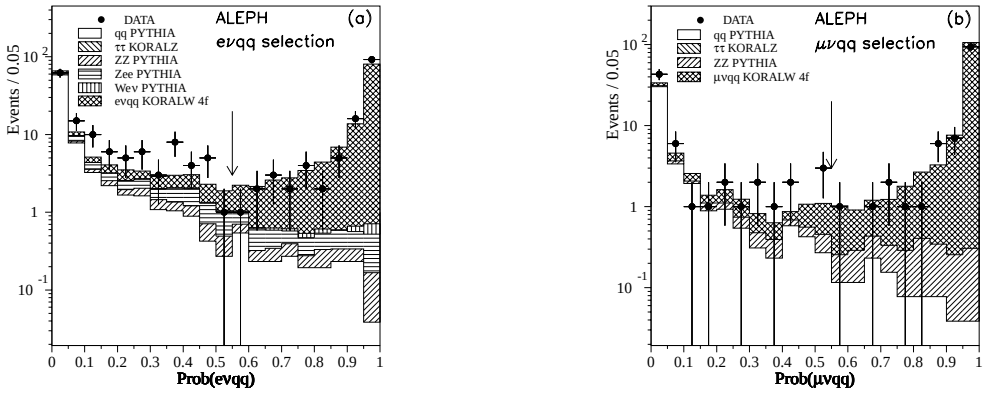

Figure 25: The probability distributions for the selection of $e\nu qq$ and $\mu\nu qq$ WW decays in ALEPH.

		Event selection and classification										
		e e	e μ	e	μ μ	μ		e qq	μ qq	qq	qqqq	All
E. for WW ! (in %)	e e	68.2	-	8.4	-	-	-	-	-	-	-	76.6
	e μ	0.1	70.8	2.0	-	2.9	0.3	-	-	-	-	76.1
	e	4.3	3.8	57.9	-	0.1	3.5	0.3	-	-	-	69.9
	μ μ	-	-	-	71.1	4.7	0.2	-	-	-	-	76.0
	μ	-	4.1	0.2	3.9	61.7	1.5	-	0.6	-	-	72.0
		-	0.7	5.1	0.3	5.6	45.2	-	-	-	-	56.9
	e qq	-	-	-	-	-	-	81.2	0.3	6.2	-	87.7
	μ qq	-	-	-	-	-	-	0.2	88.6	3.5	-	92.3
	qq	-	-	-	-	-	-	3.1	3.3	54.1	-	60.5
	qqqq	-	-	-	-	-	-	0.1	-	0.1	84.3	84.5
Backgrounds (in pb)		0.02	0.01	0.05	0.01	0.02	0.05	0.11	0.05	0.11	1.24	1.67
Observed Events		6	14	18	8	11	4	127	113	86	432	818

Figure 26: ALEPH efficiencies and backgrounds for WW events at 183 GeV c.m. energy [35].

nels j enter in the likelihood

$$\prod_i P(N_i, n_i)$$

where P is the Poisson probability of observing N_i events in channel i when n_i are expected. The n_i are given by,

$$n_i = L \times (\sum_j \epsilon_{ij}\sigma_j + \sigma_i^{bckg})$$

where L is the luminosity, σ_j the parameters we want to determine, and the σ_i^{bckg} and efficiencies ϵ are computed from the table of Fig. 26. One can also derive the σ_j from the total cross-section and the luminosity, assuming SM branching ratios for the W. In this case the total production cross-section is the only parameter.

The latest results, combining the four LEP experiments together, were also presented at the EPS-HEP-99 conference [43,1] and are shown in Fig. 28. The data clearly require the existence of the ZWW vertex, as predicted by the SM. In fact the γ, Z and t-channel ν_e excahge diagrams of fig. 21 diverge when considered separately, but the sum does not. This is shown in Fig. 28 by the dotted lines.

7. W branching ratios and measurement of $|Vcs|$

From the above measurements it is also possible to extract the leptonic and hadronic branching fractions of the W (e.g. from table of Fig. 26).

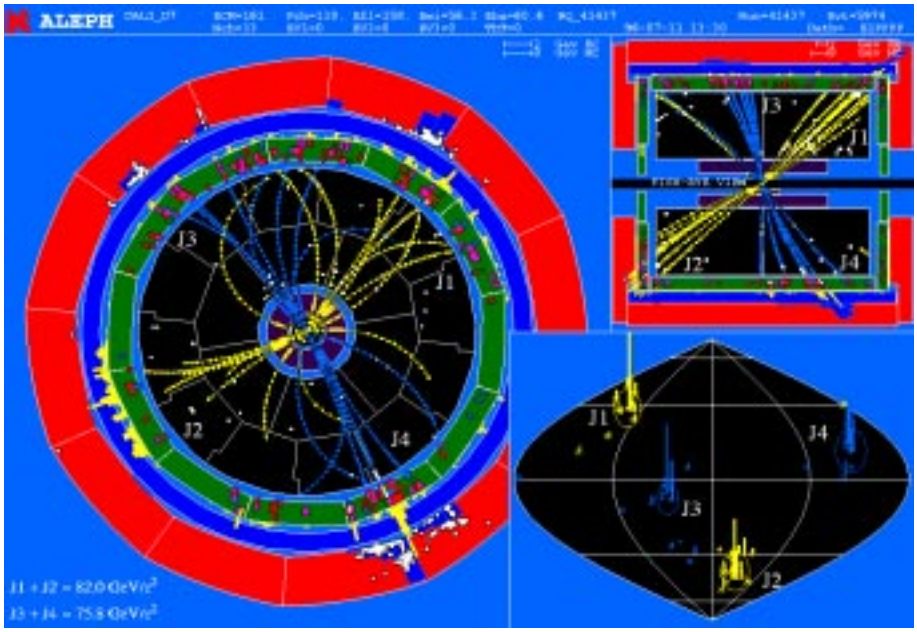

Figure 27: An example of a WW event where both Ws decay into two jets as seen in the ALEPH detector.

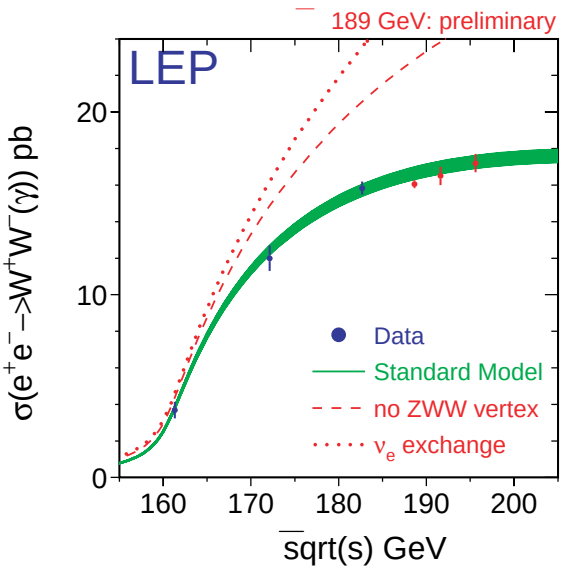

Figure 28: The WW cross-section for the four LEP experiments combined, as a function of the center of mass energy [3].

The latest measurements are shown in Figs. 29, taken again from [43,1].

In these figures the prediction of the SM is also shown. The measurement of the three independent leptonic branching ratios tests lepton universality in the weak charged current at the W mass scale:

$$\begin{aligned} g_\mu/g_e &= 1.001 \pm 0.016 \\ g_\tau/g_e &= 1.010 \pm 0.022 \\ g_\tau/g_\mu &= 1.008 \pm 0.021 \end{aligned}$$

As it can be seen the data are indeed consistent with lepton universality. The ratio g_τ/g_e has also been recently measured directly by the $D0$ collaboration with the value $g_\tau/g_e = 0.98 \pm 0.03$ [44].

Assuming Lepton Universality

$$B_e = B_\mu = B_\tau = (1 - B_{q\bar{q}})/3$$

the data described in the previous section can be fit simultaneously to the cross-sections (at each energy) and $B_{q\bar{q}}$.

The result can be put in terms of the CKM matrix elements

$$\frac{B(W \to qq)}{1 - B(W \to qq)} = (1 + \frac{\alpha_s(m_W^2)}{\pi}) (|V_{ud}|^2 + |V_{cd}|^2 + |V_{us}|^2 + |V_{cs}|^2 + |V_{ub}|^2 + |V_{cb}|^2)$$

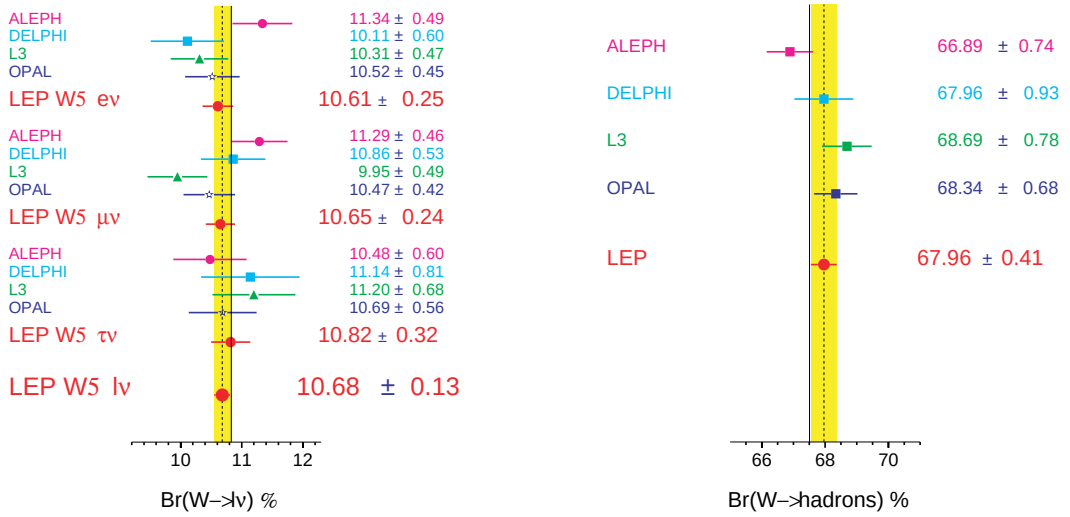

Figure 29: The W leptonic and hadronic branching ratios for the four LEP experiments together.

This relation follows from the calculation of the width of the W. In fact, the calculation within the SM of the partial widths into a particular fermion-pair final state is simple and given by

$$\Gamma^{Born}_{W\to f_i,f'_j} = N_c^f \frac{\alpha}{6}\frac{m_W}{2s_W^2}|V_{ij}|^2 F(m_{f_i}, m_{f_j}, m_W)$$

where s_W stands for the sine of the electroweak mixing angle, N_C is the color factor (1 for f=lepton and 3 for f=quark) and V_{ij} is the element of the Cabbibo-Kobayashi-Maskawa matrix for the flavor indexes i and j. The function F is equal to 1 if the fermion masses are neglected with respect to the W mass. For leptons $V_{ij} = \delta ij$. For quarks the possible pairs $(f_i, \bar{f}_j)$ are $(u,\bar{d}), (u,\bar{s}), (c,\bar{d}), (c,\bar{s})$, and the strongly Cabbibo-supressed $(u,\bar{b}), (c,\bar{b})$. After summing over all of them the total width is

$$\Gamma^{Born}_{tot} = \frac{3\alpha}{2}\frac{m_W}{2s_W^2}.$$

Radiative corrections can be conveniently included by expressing the width in terms of m_W and G_μ, giving Improved Approximation [3] widths:

$$\Gamma^{IBA}_{W\to\nu_i l_j} = \frac{G_\mu M_W^3}{6\sqrt{2}\pi}$$

$$\Gamma^{IBA}_{W\to u_i d_j} = \frac{G_\mu M_W^3}{2\sqrt{2}\pi}|V_{ij}|^2\left(1+\frac{\alpha_s(M_W^2)}{\pi}\right)$$

$$\Gamma^{IBA}_{W_{bot}} = \frac{3G_\mu M_W^3}{2\sqrt{2}\pi}\left(1+\frac{2\alpha_s(M_W^2)}{3\pi}\right)$$

from which the above expression follows.

From the world average values of $\alpha_s(m_W^2)$ (evolved from $\alpha_s(m_Z^2)$), together with other measured CKM matrix elements, a value for the least well measured $|Vcs|$ element can be obtained. The result at EPS-HEP-99 for the four experiments combined was [43,3]:

$$|V_{cs}| = 0.997 \pm 0.020$$

An alternative way of obtaining this number is to look at charm decays of the W. Since $W^- \to \bar{t}b$ $(W^+ \to t\bar{b}$ is forbidden by energy conservation and $W^-(W^+) \to \bar{c}b(c\bar{b})$ is strongly Cabbibo-suppressed, it is possible to tag charm decays (predominantly from $W \to cs$) and measure the corresponding BR. Assuming the unitarity of the CKM matrix this branching ratio is

$$BR(W \to\ charm) = \frac{|V_{cd}|^2 + |V_{cs}|^2 + |V_{cb}|^2}{|V_{ud}|^2 + |V_{cd}|^2 + |V_{us}|^2 + |V_{cs}|^2|V_{ub}|^2 + |V_{cb}|^2}$$

This has been done, using various methods to select charm events, by all the LEP collaborations. The latest results presented at EPS-HEP-99 are given in Table 9.

The question of whether or not the W could decay into undetected particles (e.g., low momentum charged particle below detectability) has been

	$F(W \to cX)/\Gamma(W \to had)$	$\lvert V_{cs}\rvert$
ALEPH	$0.51 \pm 0.05 \pm 0.03$	$1.00 \pm 0.11 \pm 0.07$
DELPHI		$0.91 \pm 0.14 \pm 0.05$
L3		$0.98 \pm 0.22 \pm 0.08$
OPAL	$0.47 \pm 0.04 \pm 0.06$	$0.91 \pm 0.07 \pm 0.11$

Table 9: W charm branching ratio and $|V_{cs}|$.

investigated by ALEPH [34]. The idea is that, in this case, the total width would be modified with respect to SM expectations, and this modification would affect the total cross-section in a small way, namely the visible cross-section would become

$$\sigma_{WW}^{vis} = (B^{vis})^2 \sigma_{WW}$$

where

$$B^{vis} = \frac{\Gamma_W^{vis}}{\Gamma_W^{vis} + \Gamma_W^{invis}} = 1 - B^{invis}$$

ALEPH made a fit to the measured cross-sections at 161, 172 and 183 GeV, taking the visible width from the SM and m_W from the world average (excluding LEP). The results were

$$\begin{aligned} \Gamma_W^{invis} &= 30^{+52}_{-48}\ (stat.) \pm 33(syst)\ MeV \\ \Gamma_W^{invis} &< 139\ MeV\ at\ 95\%\ CL \\ B^{invis} &< 6.5\%\ at\ 95\ CL. \end{aligned}$$

8. Investigation of anomalous tri-linear couplings VWW $(V = \gamma, Z)$

The triple gauge couplings in the SM (Fig. 30) are a consequence of the non-abelian structure of the electroweak interaction.

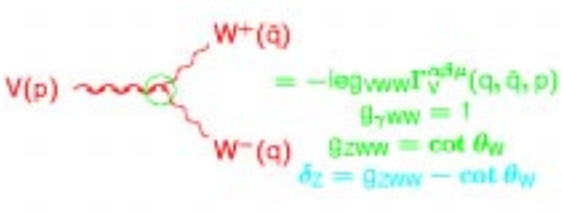

Figure 30: The VWW vertex, where V is a photon or a Z boson.

The measurement of the WW cross-section clearly establishes their existence, as we have seen above. The exact form of the couplings also has an effect on the production angles of the Ws and on their polarization (and therefore on the angular properties of their decay products).

One would like to investigate if other couplings, different from those of the SM, are also present. The most general way of writing the cross-section (compatible with Lorentz-invariance and U(1) gauge invariance) is in terms of 14 couplings. Of the 14 only 5 preserve C and P and are likely to play a role at LEP-2 (see refs. [45] to [55]):

$$g_1^Z, k_\gamma, k_Z, \lambda_\gamma, \lambda_Z$$

(In the SM $g_1^z = k_z = k_\gamma = 1$, and all the others are 0).

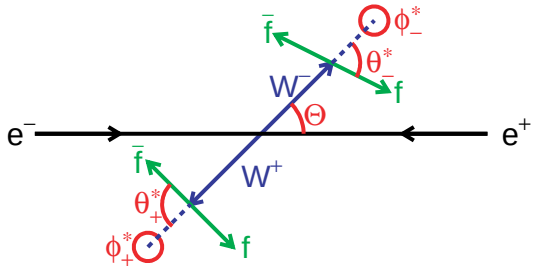

Figure 31: The angular variables used in the analysis of the triple gauge couplings.

The $W - W - \gamma$ couplings are related to the magnetic-dipole moment and the electric-quadrupole moment of the W:

$$\begin{aligned} \mu_W &= \frac{e}{2m_W}(g_1^z + k_\gamma + \lambda_\gamma) \\ q_W &= -\frac{e}{m_W^2}(k_\gamma - \lambda_\gamma). \end{aligned}$$

LEP1 measurements constrain the deviation of the couplings from their SM values (they enter in LEP-1 observables through loop-corrections). To look for deviations one tries to extract from the data

$$\Delta g_1^z = 1 - g_1^Z,\ \Delta k_\gamma = 1 - k_\gamma,\ \lambda_\gamma$$

which should be zero in the SM.

The relevant observables to measure the anomalous couplings are:

- Cross-section and production angles of Ws.
- Polar angle of decay charged-lepton or d-type quark with respect to the flight direction of the corresponding W in the rest frame of the W (see Fig. 31).
- Azimuthal angle (as above) with respect to the plane formed by the W direction and the beam.

The reconstruction of these angles is different for semi-leptonic or hadronic decays. In hadronic decays there is the ambiguity of which of the four jets belongs to the d-type quark. Overall kinematic fitting of the event is always done, to improve the resolution on the angles.

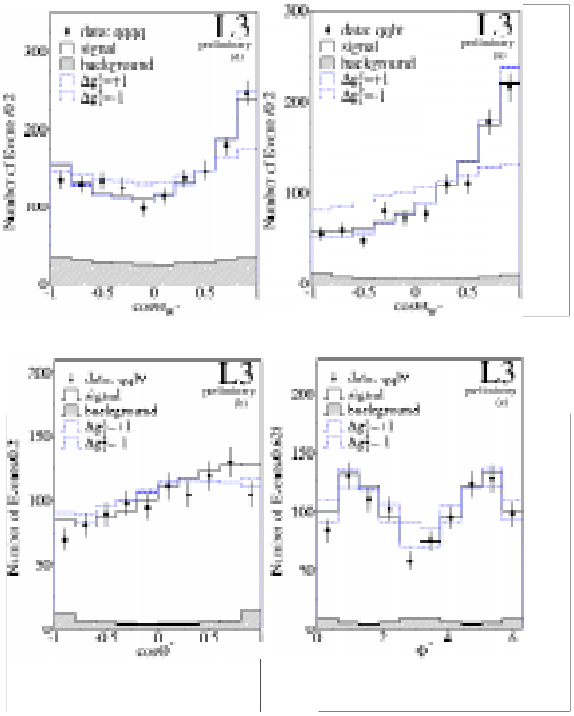

Figure 32: The distributions of the angular variables for the analysis of the trilinear couplings obtained by the L3 collaboration.

The LEP collaborations have tried several methods of fitting:

- Maximum likelihood: the probability of occurrence of an event with the measured variables at each energy can be calculated by MC simulation, taking the measured cross-section for the corresponding energy. The problem with this method is how to introduce background and detector effects. This problem can be avoided with a binned likelihood method, but the statistics is very limited to proceed in this way.
- Another technique is that of the "Optimal Observable". For a given anomalous coupling α_i, the cross-section can be written as

$$\frac{d\sigma}{d\Omega} = C_0^i(\Omega) + C_1^i(\Omega)\alpha_i + C_2^i(\Omega)\alpha_i^2$$

The quantity C_1/C_0 (computed after folding-in ambiguities) is the optimal observable (OO) for α_i and can be computed for each event j. A maximum likelihood fit can then be performed to obtain α_i:

$$lnL = \sum_{j=1}^{n} lnP(00_i^j, \alpha_i)$$

To show the sensitivity of the angular variables to anomalous couplings the results of L3 at 189 GeV are shown in Fig. 32, and the results from the four LEP experiments, together with the form of the likelihood functions, in Fig. 33 [3].

9. W boson longitudinal polarization

Unlike the massless photon, which has only two helicity states, the massive W and Z bosons have three polarization states, two transverse, like the photon, and one longitudinal. This state arises from the electroweak symmetry breaking mechanism, and its study is of importance at LEP and at future linear colliders. For the highest energies of LEP the fraction of longitudinally polarized W's produced in WW events becomes substantial.

The polarization of the W's can be inferred from the angular distribution of the lepton in leptonic W decays or the quark in hadronic decays. For transversally polarized W's the distribution of the angle in the W rest frame with respect to the W laboratory line of flight, θ^*, goes as

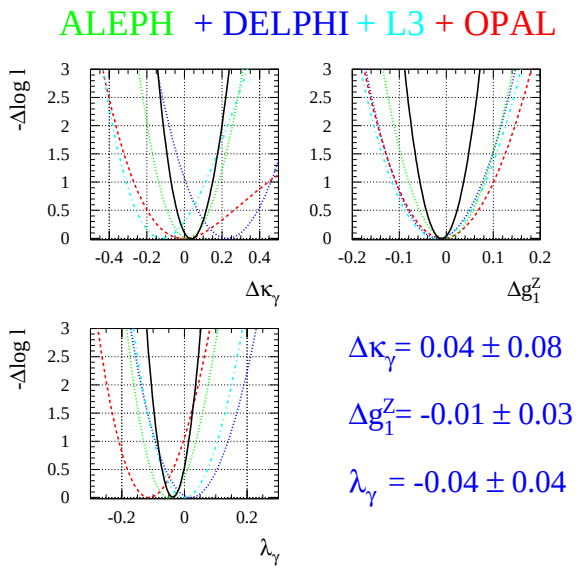

Figure 33: The values of the anomalous couplings resulting from the four LEP experiments. To obtain each value it is assumed that the other two couplings have the SM value. Each of the curves in the plots is for a different LEP experiment [3].

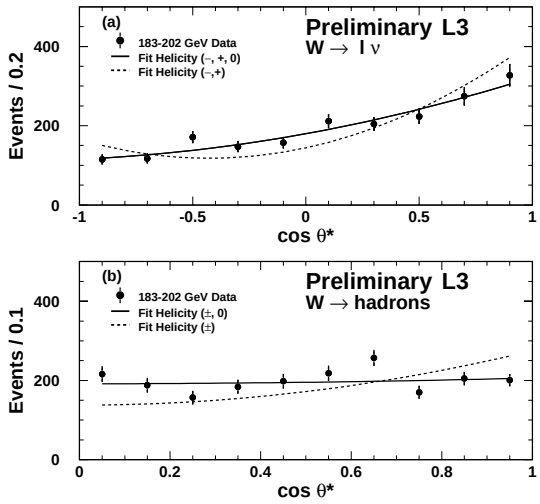

Figure 34: Polar angle of the charged lepton (top) and of the jet (bottom) in the W rest frame for leptonic and hadronic W decays in WW events. The curves indicate the expectations allowing different polarization states, as indicated [1].

$(1 + \cos\theta^*)^2$ while for longitudinally polarized W's the distribution is proportional to $\sin^2\theta^*$.

All the LEP collaborations are studying this topic. Data from L3 are shown in Fig. 34.

The measured fraction of longitudinally polarized W's is $0.285 \pm 0.053 \pm 0.03$ which is in agreement with the SM prediction at the 1σ level.

10. Single W production

W bosons can also be singly produced by the diagram of Fig. 35. The final state electron typically stays inside the beam pipe and the only visible particles are those coming from the W decay.

This reaction is being studied by all the LEP collaborations. Shown in Fig. 36 are data from L3 and ALEPH, compared with SM predictions. As it is clear from the diagram, the reaction also proceeds via a triple boson coupling and thus can be used to study possible anomalous couplings [56].

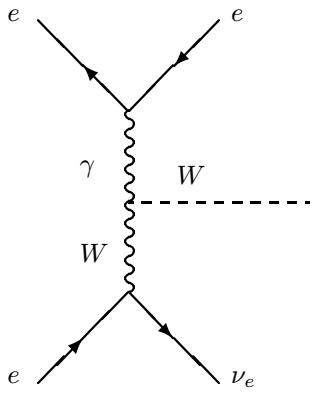

Figure 35: Single W production diagram.

11. Measurement of the W mass

This is one of the most important measurements in LEP-2 and it has been extensively studied by all the LEP experiments [57]-[67]. The measurements of the W-mass starts with the selection of WW events as explained section in section 6.

Once we have these events, there are three

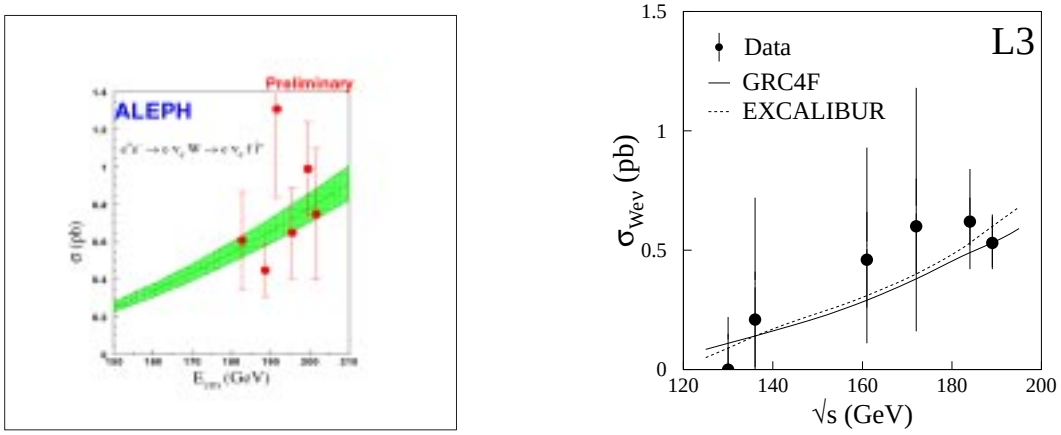

Figure 36: The single W production cross-section for several center of mass energies from ALEPH and L3. The curves are SM Monte Carlo calculations.

different methods to measure the mass:

1. Measurement of the end-point of the charged lepton spectrum in semileptonic W decays. This is a classical method of measuring masses. It is clean and easy to interpret, but limited statistically, and we do not describe it further.

2. Measurement of the WW cross-section near threshold. Near the WW threshold the WW production cross-section is sensitive to the value of the W mass. The advantage of this method is that all decay modes can be used. But one needs to run very close to threshold, and therefore the statistics are limited and the background large.

3. Direct reconstruction. The mass can be directly obtained from the reconstruction of the W decay products. This is the most appropriate method above threshold. It uses most of the decay channels, but for 4 jet events there are soft QCD effects that have to be taken into account.

For all the methods one needs the beam energy, which is used as a constraint (see below).

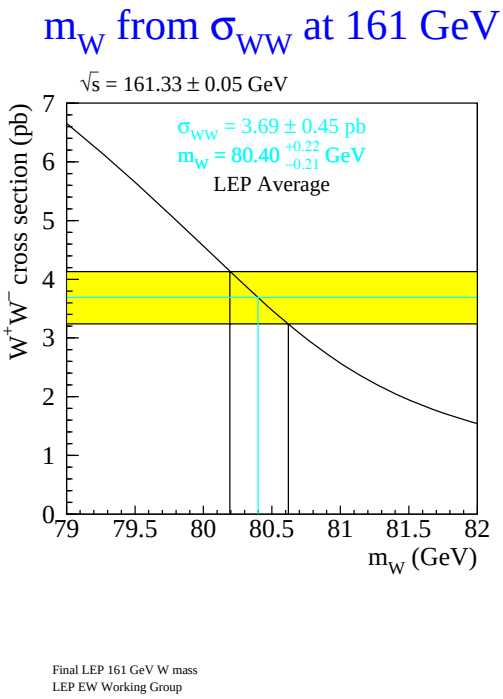

Figure 37: The W mass from the WW threshold cross-section.

11.1 W-mass from the WW threshold cross-section.

The sensitivity of the cross-section to the W mass is maximum near threshold. The optimal point is at 161 GeV center of mass energy, which was chosen as one of the points for running LEP-2 because of this reason.

It is not simple to write the WW production

cross-section as a function of the energy since there are quite a few effects that have to be taken into account. What we want to compute is the CC03 diagrams of Fig. 21, followed by the decay of the Ws. The decay of the Ws is introduced by the convolution [68],[69]

$$\sigma^{cc03}(s) = \int_0^s ds_+ \rho_W(s_+) \int_0^{(\sqrt{s}-\sqrt{s_+})^2} ds_- \rho_W(s_-)\sigma_0^{cc03}(s, s_+, s_-)$$

where the ρs are Breit-Wigner functions for non-zero width Ws,

$$\rho_w(s_\pm) = \frac{1}{\pi}\frac{m_W\Gamma_W}{|s_\pm - M_W^2 + im_W\Gamma_W|^2}BR$$

and where the s are the invariant masses of the internal Ws, and BR the branching ratio of the specific final state considered. The σ_0 inside the integral is the cross-section corresponding to the CC03 diagrams of Fig. 21 and their interference. It is given by the expression

$$\sigma_0^{cc03}(s^0, s_+, s_-) = \frac{(G_\mu m_W^2)^2}{8\pi s}\times$$
$$[(c_{\gamma\gamma} + c_{\gamma Z} + c_{ZZ})G^s(s, s_+s_-)+$$
$$+(c_{\nu\gamma} + c_{\nu Z})G^{st}(s, s_+s_-) + (c_{\nu\nu})G^t(s, s_+s_-)]$$

where the c's are functions of the coupling constants and propagators indicated by their labels and the Gs depend on the kinematics.

The radiative corrections to these expressions are difficult to introduce, mainly because they do not factorize into photonic and weak corrections as in LEP-1. Adequate approximations exist nevertheless to introduce the main effects. These are

- Initial state radiation. They are included by introducing a "flux function" (or an structure function) which plays a role analogous to the radiator function used in the analysis of LEP-1 data.
- Coulomb singularity. At threshold the two Ws are produced almost at rest and move slowly. The approximation that they are free particles is no longer adequate since they are affected by the long range electromagnetic interaction. This is included as a correction consisting on the change

  $$\sigma_0^{cc03}(s) \to C_0^{cc03}(s)(1 + \delta_C(s, s_+, s_-))$$

  where δ_C is a function of the kinematics. At 161 GeV it represents a correction of the cross-section of 5.7 %.
- Improved Born Approximation. The treatment here is again more complicated than at the Z, since the W mass appears both in the matrix element and in the phase space factor. The so-called fixed width scheme is used [3].

There are other final-state effects, namely color-reconnection and Bose-Einsten correlations, which affect the cross-section but which are not important for the measurement at threshold. However, they have a substantial effect in the direct determination of the mass from the jet reconstruction and are described in the next section.

The dependence of the WW cross-section, at the fixed energy of 161 GeV in the center of mass, as a function of the W mass is shown in Fig.37. The band in that figure is the measured cross-section averaged over the four LEP experiments and the resulting one-sigma value of the W mass. The values are also shown in the plot.

11.2 W-mass from direct reconstruction.

The mass can also be reconstructed directly from the kinematics of the W decays. There are three different "channels" to calculate the mass:

(A) Leptonic: $W^+W^- \to l^+\bar{\nu}l^-\nu$.

In this case the system is underconstrained (due to the 2 neutrinos) and the precision on the mass is small.

(B) Semi-leptonic: $W^+W^- \to l\nu q_1\bar{q}_2$.

Here events are selected where one W decays semileptonicaly the other in $q_1\bar{q}_2$. These events are typically selected with high efficiency (80% for e and μ semileptonic decays, 40% for τ) and low backgrounds (less than 5%). The mass resolution is improved

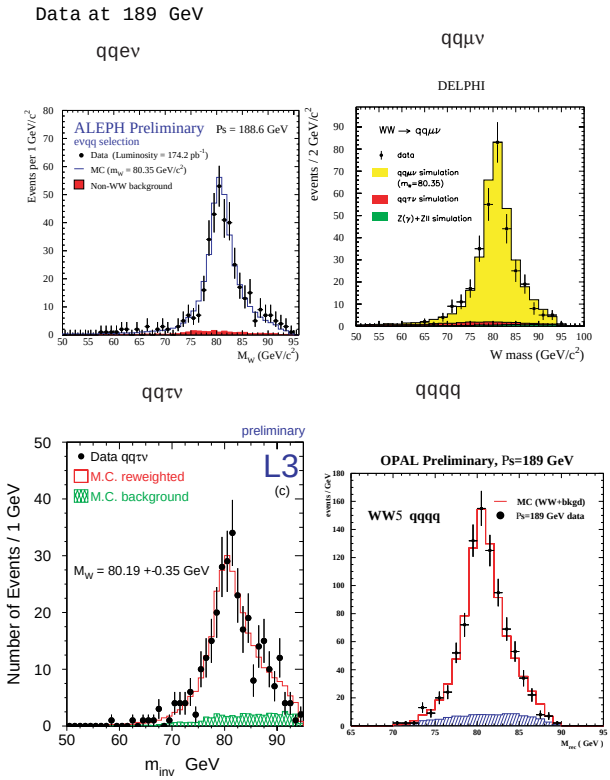

Figure 38: Effective masses for different final states from the four LEP experiments [3].

by imposing, through a fit, energy-momentum conservation (a 2-c fit in this case).

(C) hadronic: $W^+W^- \to q_1\bar{q}_2q_3\bar{q}_4$

In this case both W's decay to $q_1\bar{q}_2$, and the final state is a typical 4-jet event. As one has to avoid the "non-resonant" and "radiative return" backgrounds the efficiency is smaller than for the semileptonic case (70% typically) and the background higher (15% typically). However, the statistics is high.

Here a 4-c fit can be imposed to improve jet energy and angular resolution, and thus mass resolution. Other fits can also be imposed (e.g. equal reconstructed masses on both jet pairs).

An additional problem in this case comes from jet pairing. The four jets can be paired into two di-jets in 3 different ways. The way this is handled (e.g. in ALEPH [58]) is by choosing as the right combination that which gives the smallest different between the two masses reconstructed from each di-jet, unless this combination has the sum of the two di-jets opening angles, in which case the combination with the second smallest mass difference is selected. At the end a comparison is made with a Monte Carlo sample, treated in the same way as the data, and this decreases the importance of the exact procedure followed to select the events.

The invariant mass distributions reconstructed from the 4 jet final state should have a Breit-Wigner form, which is however distorted due to many effects, such as initial state radiation, detector resolutions, wrong assignment of particles to jets and others. See [70] for a review of the measurements presented at EPS-HEP-99.

All the LEP experiments have developed methods to handle this problem. The most common is to compare measured di-jet mass distributions with MC generated samples with different masses, and choose as the value of the W mass that used to generate the MC events that best resemble the data. The problem is how to avoid the generation of many Monte Carlo samples. The procedure is that of the "re-weighting technique" which goes as follows: a large sample of Monte Carlo events is generated at a given reference mass, m_W^{ref}. This sample of Monte Carlo events is used again and again, each time with a weight for every event given by

$$w_i(m_W,\Gamma_W) = \frac{|m(m_W,\Gamma_W,P_i^1,P_i^2,P_i^3,P_i^4)|^2}{|m(m_W^{ref},\Gamma_W^{ref},P_i^1,P_i^2,P_i^3,P_i^4)|^2}$$

where M represents the matrix element of the $CC03$ diagrams at the given value of m_W and Γ_W, and the p_i^j is the four momentum of fermion j (of the jet in the quark case) of the four-fermion final state for event i. The W-mass distribution of the samples are compared with the data until the best match is found. The corresponding m_W mass is the best estimate of the real W mass.

Technically one makes probability distribution functions (p.d.f.) from weighted MC events in which the non-weighted background is also included. From this p.d.f. a likelihood function for

the data can be constructed and a mass obtained from its maximization. The re-weighting can be applied to the two di-jet masses independently, thus properly accounting for the event by event correlations. This gives an improvement of the statistical error of about 10% with respect to one mass alone [59],[71].

Shown in Fig. 38 are the effective masses of different final states from the four LEP experiments, and their comparison with the corresponding Monte Carlo.

For the 4-quark final state there are two additional problems, as mentioned above, namely:

- Color reconnection. In the four-quark final-state it is possible that the two original color singlets interact strongly and exchange color before hadronization. The effect has been investigated by comparing the jet charged multiplicities of $qqqq$ final states with those coming from semileptonic final states $qql\nu$. The latter should not be affected by the color-reconnection problem. The data are compatible with small or no effect. The estimated contribution to the systematic error on the W mass is 25-70 MeV [70].

- Bose-Einstein correlations. At short distances there could be correlations between the low-momentum identical bosonic particles such as neutral pions, leading to an enhancement of their production. This would lead to momentum transfer between the decay products of the two bosons, and hence distort the invariant mass. These correlations have been indeed established by OPAL in hadronic Z decays and in decays of the same W [1]. The estimated systematic error on m_W is 20-60 MeV [70].

The error on the beam energy enters directly into the the error of the W mass, through the kinematic fits:

$$\Delta m_W/m_W = \Delta E_b/E_b$$

At present the beam energy is determined by the resonant depolarization technique at the Z, and then extrapolated to the higher energies [72]. The error at $\sqrt{s} = 183\ GeV$ is $\Delta E_b = \pm 50 MeV$. This error has already a substantial impact on the final precision.

The results of the four LEP experiment and their averages are shown in Fig. 39 for the 4-quark and semileptonic final states. The combined result from LEP is

$$m_W = 80.350 \pm 0.056\ GeV$$

It should be compared with those obtained at the Tevatron, by CDF ($m_W = 80.433 \pm 0.079$ GeV) and D0 ($m_W = 80.482 \pm 0.091$ GeV) [73].

12. Standard Model Fits

The measurement of the W mass, both from LEP and from the Tevatron, adds one more important observable to those already described in section 2, that allows tests of the Standard Model additional to those described in section 2.5.

A first check of consistency comes from fitting all data, in the context of the SM (using ZFITTER or TOPAZ), leaving as parameters m_Z, m_t, m_H, α and α_s, that is, as indicated by the last equation of section 2.4, where G_F is fixed to the value obtained in muon decay, $G_F = 1.16639(2) \times 10^{-5}$ GeV^{-2}, the light fermions masses fixed to their values, and their influence on the main error on α introduced in $\Delta\alpha^{(5)} = 0.02804 \pm 0.00065$, also kept "fixed" to this value. The fit [3] gives $23/15\ \chi^2/d.o.f.$, m_Z and α do not vary appreciably from their input values, and

$$\begin{aligned} m_t &= 173.2 \pm 4.5 GeV/c^2 \\ m_W &= 80.385 \pm 0.022 GeV/c^2 \\ m_H &= 77^{+69}_{-39} GeV/c^2 \\ \alpha_s(m_Z^2) &= 0.118 \pm 0.003 \end{aligned}$$

The minimun of the χ^2 as a function of m_H is shown in Fig. 40. The minimum is at the indicated value of m_H but the dependence on the Higgs mass is only logarithmic. It is more appropriate to quote the result

$$log\ (m_H/(GeV/c^2)) = 1.88^{+0.28}_{-0.30}$$

We have

$$m_H < 245\ GeV/c^2\ at\ 95\%\ CL$$

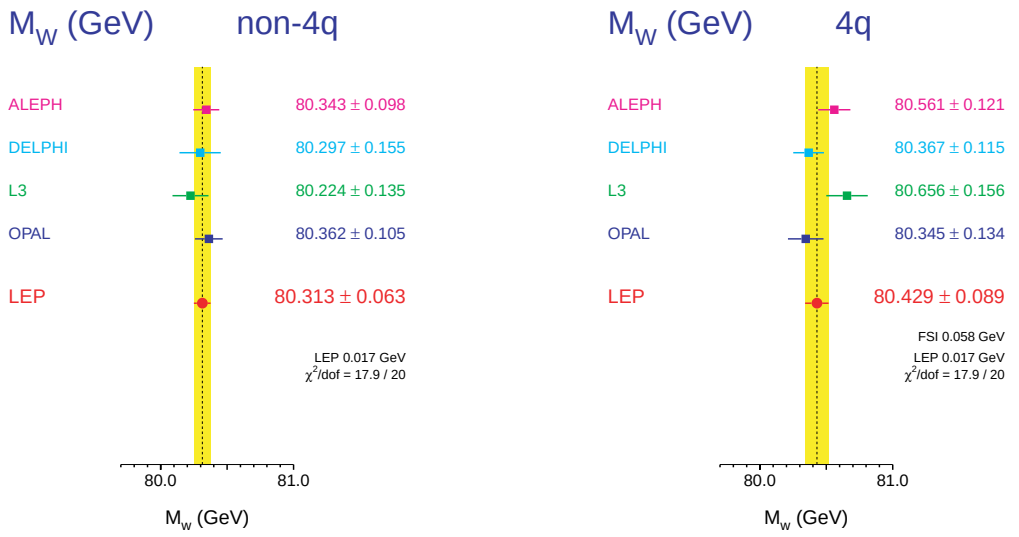

Figure 39: The W mass for four-jet final states and for other but entirely hadronic final states.

and the upper bound moves up very quickly if we go above 2 standard deviation limits.

With the 5 fitted parameters one can then predict the value of all the observables and compare with the measured values. The deviations between the measured and fitted observables, normalized to their fitted values (the "pulls") are shown in Fig. 41, at the time of the 1999 Lepton Photon Symposium [74].

Other fits are those of Table 10 [3]. The first colum shows the results when only LEP data are used. In particular the value obtained for the top mass, 172^{+14}_{-11} GeV, agrees very well with the value $m_t = 174.3 \pm 5.1$ measured directly at the Tevatron. This confirms the validity of the electrweak radiative correction calculations.

The third colum gives the results when all measurements, except for the W mass, are used. In this case one obtains the value $m_W = 80.381 \pm 0.026$, which should be compared with its direct determination at LEP and the Tevatron, shown in the table. Again, the direct and indirect determinations are in good agreement. The W thus exists as a real particle and as a gauge boson whose mass, together with that of the Z, gives the correct couplings.

Fig. 42 shows the 68% contour of the direct measurements of m_W versus m_t (Tevatron and LEP-2, dashed contour) and the indirect determination (from LEP-1+SLD+νN, solid curve). The shaded band is the SM relationship between m_W and m_t. The 3 lines inside correspond to $m_H = 95, 300, 1000\ GeV/c^2$ as shown. Again the data favor a small Higgs mass.

13. Searching for the Standard Model Higgs Boson

We have seen in the above sections how well the Standard Model works, explaining consistently the data obtained at LEP and elsewhere. But it is a fact that the $SU(2)_L \bigotimes U(1)_Y$ symmetry of the electro-weak theory is broken: the photon is massless while the Z and W bosons are very massive, and all the fermions have mass (except, perhaps, the neutrinos). Understanding the mechanism for this breaking, the origin of mass, remains as one of the fundamental problems in particle physics. The simplest breaking mechanism is that of the Standard Model itself: a com-

	LEP including LEP-II m_W	all data except m_W and m_t	all data except m_W
m_t [GeV]	172^{+14}_{-11}	167^{+11}_{-8}	172.9 ± 4.7
m_H [GeV]	134^{+268}_{-81}	55^{+84}_{-27}	81^{+77}_{-42}
$\log(m_H/\mathrm{GeV})$	$2.13^{+0.48}_{-0.40}$	$1.74^{+0.40}_{-0.30}$	$1.91^{+0.29}_{-0.32}$
$\alpha_s(m_Z^2)$	0.120 ± 0.003	0.118 ± 0.003	0.119 ± 0.003
$\chi^2/d.o.f.$	11/9	21/12	21/13
$\sin^2\theta^{lept}_{eff}$	0.23184 ± 0.00021	0.23151 ± 0.00017	0.23152 ± 0.00018
$1 - m_W^2/m_Z^2$	0.2237 ± 0.0006	0.2233 ± 0.0007	0.2230 ± 0.0005
m_W [GeV]	80.342 ± 0.032	80.366 ± 0.035	80.381 ± 0.026

Table 10: Electroweak fits described in the text [3]. The bottom parameters are derived quantities.

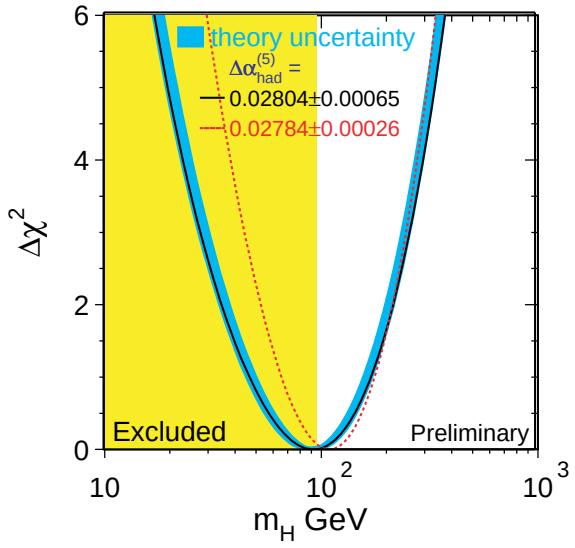

Figure 40: The line in the figure is the $\chi^2 - \chi^2_{min}$ from a fit to all the electroweak data of LEP and the Tevatron. The central value of the Higgs mass is below the exclusion limit from direct searches, which is $95.2 GeV/c^2$ at 95% CL (shaded area). The 95% CL upper level from the fit is $245 GeV/c^2$ [3].

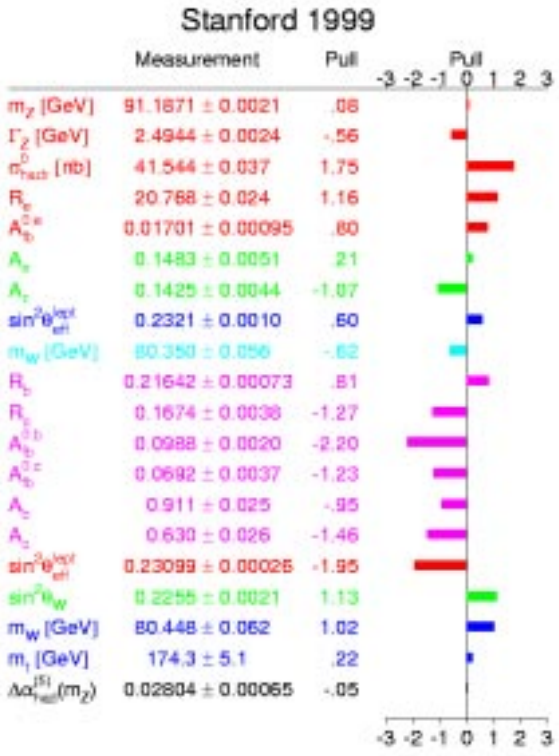

Figure 41: The measurements used to fit the SM, and their pulls with respect to the SM fit explained in the text.

plex iso-doublet field which spontaneously breaks the symmetry by acquiring a non-zero expectation value. The masses of the particles are generated by their Yukawa-like interactions with the field. Three of the four components are "used" to create the longitudinal components of the Ws and the Z, while the remaining fourth manifests itself as a neutral particle: the Higgs. This is a Minimal Standard Model, and it is very appealing esthetically.

The Yukawa-like interactions implies that the Higgs couples to fermions proportionally to their masses, which is one of the fundamental properties that has to be proven if the Higgs is found. Although the mass of the Higgs is not given by

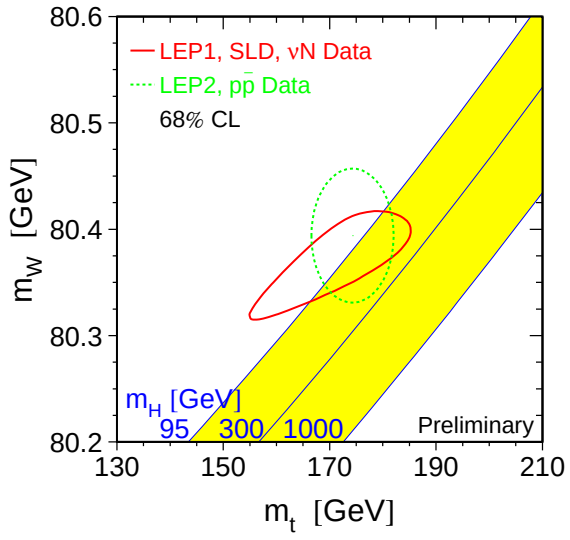

Figure 42: Comparison of the direct (dashed curve) and indirect (solid curve) determination of the W mass, and the SM predicted relation as a function of the Higgs mass for different Higgs masses (shaded area) [3].

the model, it can be severely constrained by theoretical considerations (see for example references [15], [75], [76], [77]).

Consistency conditions within the SM restrict the mass of the Higgs to values below 1 TeV, while a lower bound on the mass follows from the requirement that the vacuum be stable. The lower bound depends on the top mass and on the scale Λ up to which the SM can be extended before the emergence of new strong interactions of the fundamental fermions. An upper bound also follows from the requirement that the SM be valid up to the scale Λ,

$$m_H^2 \leq \frac{8\pi v^2}{3log\frac{\Lambda^2}{v^2}} \quad v \approx 246 GeV/c^2.$$

If we take Λ up to the Plank scale the limits are

$$130 GeV/c^2 < m_H < 190 GeV/c^2$$

but these limits change if we move Λ.

As we have seen earlier, precision measurements of electro-weak observables (particularly at LEP-1) constrain the possible values of the SM Higgs mass, but given the logarithmic dependence the resulting values of the Higg mass are not very restrictive. Direct searches exclude the SM Higgs with masses below 95.2 GeV/c^2 as we will see.

The dominant process for the production of the SM Higgs at LEP-2 is the "Higgs-strahlung" process, Fig. 43, where the Higgs couples to the highest mass particle available, the Z. However, for the highest energies the fusion processes, also depicted in Fig. 43, start to contribute.

When

$$m_H \geq \sqrt{s} - m_Z$$

the Higgsstrahlung cross-section drops sharply. This can be seen in Fig. 44, which shows, on the left, the cross section for Higgs production as a function of the Higgs mass for three different LEP c.m. energies.

This is different from what happens in hadron machines, like the LHC, where the collisions, at fixed beam energies, involve a very wide range of energies at the parton level. Let's take a numerical example: at $\sqrt{s}$ = 198 GeV and m_H =100 GeV/c^2, the HZ cross-section is about 0.25 pb. If the integrated luminosity reaches $200 pb^{-1}$, each LEP experiment will collect 50 events. However, one has to reject the ZZ events and other background, which is important when the ZZ channel opens, Fig. 44. This translates in an inefficiency of selecting HZ candidates.

For Higgs masses in the region of interest for LEP2 (e.g. 90 to 110 GeV/c^2) the Higgs decays mainly into $b\bar{b}$ (85%) and much less so into $\tau^+\tau^-$ (8%) and $c\bar{c}$ (4%), and these branching ratios are almost independent of the mass, for masses around 100 GeV. The H width is small (e.g. less than 3 MeV for m_H less than 100 GeV/c^2). The search strategies are based on the characteristics of these decays, together with those of a *real* Z.

All the LEP experiments have searched for the Standard Model Higgs boson at LEP-2 [78]-[88] (and at LEP-1). There are four different decay channels to look for which are explained in the next four subsections.

13.1 The muon and electron channel

The final state topologies to look for are those of

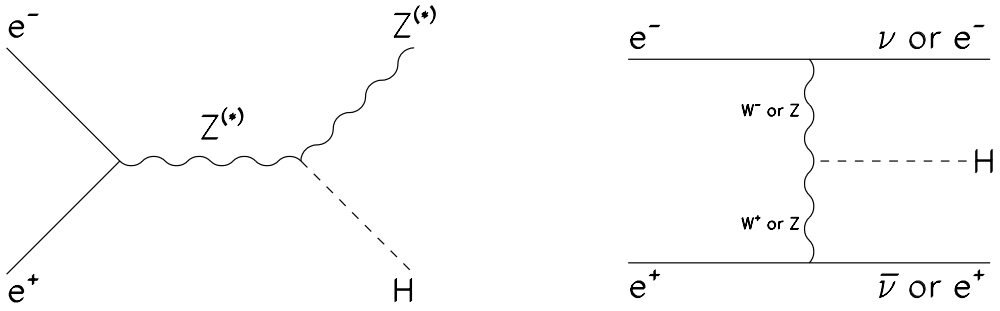

Figure 43: Feynman diagrams for the Higgs-strahlung and fusion (ZZ and WW) processes.

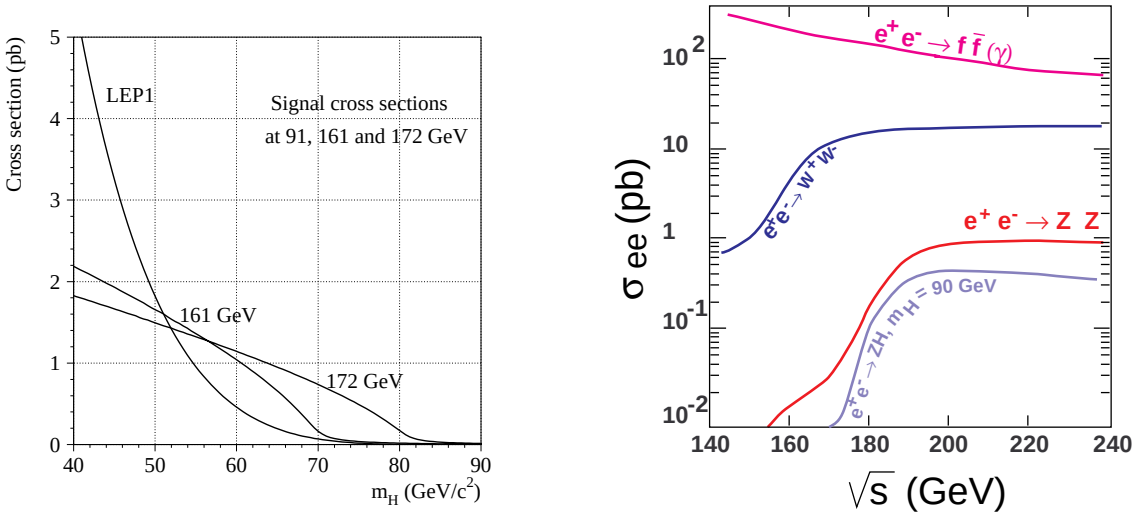

Figure 44: On the left the cross-section for Higgs production as a function of the Higgs mass, for three LEP center of mass energies. On the right the cross-section for several processes as a function of the center of mass energy.

are

$$Z \to l^+l^- \ (l = e, \mu)$$
$$H \to jet - jet$$

This channel comprises 6.7% of all the Higgs final states (the e^+e^- channel has a small contribution from ZZ fusion).

The main selection criteria for this channel are:

- The lepton invariant mass should be close to the Z mass.
- The invariant mass of the system recoiling against the leptons should be large.

Therefore the events are first selected by requiring identified or isolated lepton candidates with an invariant mass close to the Z. Background from $WW \to q_1\bar{q}_2 l\nu$ events are rejected by requiring that the mass of the qq system be above the W mass. In this channel no b-tag is necessary, and the efficiency is large (about 75%).

13.2 The missing energy channel

Here one looks for final states coming from

$$Z \to \nu\bar{\nu}$$
$$H \to b\bar{b}$$

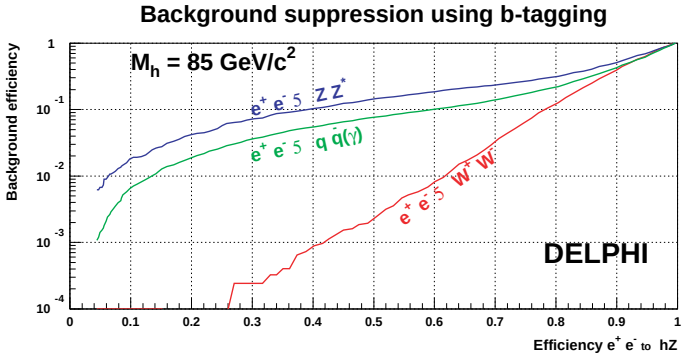

Figure 45: Background rejection power of the b-tagging technique in DELPHI. The "efficiency for selecting three background processes is shown versus the efficiency for selecting real Higgs decays.

and this channel represents 17% of the Higgs final states.

The main background for this channel are radiative-return events. The selection criteria are designed to first reject these events, for example requiring that the missing transverse momentum be in the direction of the detector (and not along the beam).

The tagging of the jets as coming from b particles is the other very powerful selection tool (see below). The b jets from these events are also acoplanar, as opposed to those coming from radiative Z events which are planar with the beam.

13.3 The tau-jets topology

The final states are

$$Z \to \tau^+\tau^-$$
$$H \to b\bar{b}$$

or

$$Z \to q\bar{q}$$
$$H \to \tau^+\tau^-$$

These events should have 4 jets, 2 of them of low multiplicity. There is also missing energy due to the neutrinos coming from the decays of the taus. The first step is to identify the tau jets. Once this is done, the b tagging is imposed to the other two jets for the first case, $\tau^+\tau^- H$. For the $H \to \tau^+\tau^-$ and $Z(\to q\bar{q})$ channel, no b-tag is possible and the selection is less efficient as more stringent cuts are adopted to select the taus.

The total fraction of Higgs events with this topology is about 9% and selection efficiencies are of the order of 20% for $\tau^+\tau^- H$ and 17% for the $q\bar{q}H$ events.

13.4 The 4-jet channel

This channel amounts to 64% of the cases, and consists on

$$Z \to q\bar{q}$$
$$H \to b\bar{b}$$

The main distinctive characteristic of these events is the 4-jet topology. The Z and H are produced almost at rest and hence the events should be "spherical". The jet isolation is one of the main discriminating variables.

Typical backgrounds are $e^+e^- \to W^+W^-$, $e^+e^- \to Z\bar{Z}$, $e^+e^- \to q\bar{q}\gamma$ and $e^+e^- \to q\bar{q}g$ where the gluon g hadronises into a jet.

The $b\bar{b}$ requirement suppresses strongly most of the above backgrounds. The $b\bar{b}$ tagging technique has been extensively studied at LEP-1 (with the aim of measuring R_b) and its importance is illustrated in Fig. 45.

14. Limits on Higgs mass

The latest data from the LEP experiments presented at the EPS-HEP-99 Conference [89],[90] are shown in Table. 11.
No significant number of events were found above what is expected from background processes.

	Luminosity	Predicted Background	Events Observed
ALEPH	176.2	44.4	53
DELPHI	158	172.7	187
L3	176.4	91.1	94
OPAL	172.1	35.4	41

Table 11: Higgs candidates expected from background processes and candidates observed in the data on the four LEP experiments [89], [90].

From the numbers on the table there remain the problem of giving a lower bound on the mass of the Higgs, combining the four LEP experiments. The issue is complicated since, on the one hand, the expected signal is well below background, and, on the other, the individual limits from the experiments, or from a single experiment but obtained with several different methods, have to be combined in a statistically consistent way (see for example [91]). Again an LEP-wide group was formed to combine the results of the four experiments [92]. The limit is obtained incorporating not only the assumed fluctuations of the number of background events, but also their characteristics (e.g. effective masses of the candidate Higgs decay products).

The limit presented at EPS-HEP-99 is

$$m_H < 95.2 GeV/c^2$$

and is shown in Fig. 40. The limit is significantly above the Z mass, that is a Higgs with a mass smaller or equal than that of the Z is strongly excluded. The limit above is actually the "observed" limit, while the "expected limit" (what one would expect assuming that there is no signal and that all we have is background with appropriate fluctuations) is 97.2 GeV/c^2. An "observed" limit smaller than the "expected", means that the data do have characteristics of a signal, that is, that the hypothesis that they are all background is not as good as it should be, statiscally speaking.

The above is indeed the remaining question: what is the minimal mass that the Higgs should have such that it could still be found at LEP-2?. The answer depends of course on the maximum energy that LEP can reach and on the integrated

Both points should be shifted 200 MeV to the left.

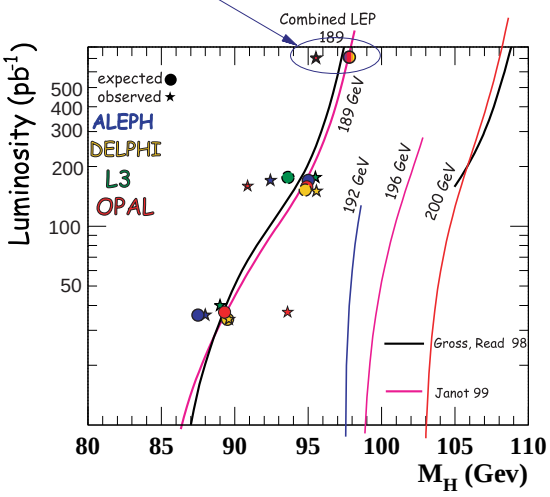

Figure 46: The luminosity required to establish a Standard Model Higgs signal at the 5σ level as a function of the Higgs mass, for the indicated center of mass energies [70].

luminosity that it can deliver. This has been investigated, for example in [91]. The conclusion is that for an integrated luminosity of 200 pb^{-1} at a center of mass energy of 200 GeV, the exclusion limit (the minimum mass of the Higgs such that the signal hypothesis can be excluded) is 109.1 GeV/c^2, while the discovery potential (the maximum mass of the Higgs such that the signal hypothesis can be established at the 5σ level) is 106.9 GeV/c^2. This is illustrated in Fig. 46 which shows the luminosity required to establish a Standard Model Higgs signal at the 5σ level as a function of the Higgs mass, for the indicated center of mass energies [89].

But LEP is running at 208 GeV, and the excluded limit will be even higher, depending on the accumulated luminosity. Or, we all wish, the Higgs could still be found at LEP!.

15. Acknowledgements

It is a pleasure to thank the organizers, particularly Enrico Nardi and William Ponce, for the invitation to give these lectures and for the very good organization of the conference, which ran

very pleasantly and, despite the circumstances, smoothly, in such a beautiful location.

16. References

1. J. Mnich, "Tests of the Standard Model", EPS-HEP-99. Proceedings of the International Europhysics Conference on High Energy Physics, held in Tampere, Finland, July 1999. Edited by K. Huitu, H. Kurki-Suonio and J. Maalampi, Institute of Physics Publishing, 2000.
2. M. L. Swartz, "Precision Electroweak Physics at the Z", talk at LP99 (the XIX International Symposium on Lepton and Photon Interactions at High Energies, held in Stanford University, USA, August 1999), hep-ex/9912026.
3. The LEP Collaborations ALEPH, DELPHI, L3, OPAL, the LEP Electroweak Working Group, and the SLD Heavy Flavour and Electroweak Groups, "A combination of Preliminary Electroweak Measurements and Constraints on the Standard Model", CERN Preprint CERN-EP-2000-016 (2000).
4. Working Group on LEP Energy, R. Assmann et al., *Eur. Phys. J.*, **C 6** (1989) 187.
5. B.F.L. Ward et al., *Phys. Lett.* **B 450** (1999) 262.
6. See reports on LEP physics: CERN 86-02 (1986), Edited by J. Ellis and R. Peccei. CERN 89-08 (1989), Edited by G. Altarelli, R. Kleiss and Z. Verzegnassi.
7. W. Hollik, "Standard Model Theory", talk ICHEP-98 and references therein. Proceedings of the 29th International Conference on High Energy Physics, held in Vancouver, Canada, July 1998). Edited by A. Astbury, D. Axen and J. Robinson, World Scientific, 1999.
8. Sirlin, "Ten years of precision electroweak physics", talk at LP99 (cf. ref. [2]), hep-ph/9912227.
9. D. Bardin, "LEP1 and LEP2 $2f$ review", in EPS-HEP-99, cf. ref. [1].
10. Program ZFITTER, D. Bardin et al. *Z. Physik* **C 44** (1989) 493, preprint DESY 99-070, and references therein.
11. Program TOPAZ, G. Montagna et al. *Nucl. Phys.* **B 401** (1993) 3, hep-ph/9804211 and references therein.
12. M. Martinez, R. Miquel, L. Rolandi and R. Tenchini: "Precision Tests of the Electroweak Interaction at the Z Pole", *Rev. Mod. Phys.* **71** (1999) 575.
13. I. Boyko, "Test of lepton universality in tau decays", in EPS-HEP-99, cf. ref. [1].
14. S. Eildelman and J. Jegerlehner, *Z. Physik* **C 67** (1985) 185
15. Physics at LEP2, eds. G. Altarelli, T. Sjostrand and F. Zwirner, CERN 96-01 (1996).
16. ALEPH Col., *Phys. Lett.* **B 378** (1996) 373
17. ALEPH Col., *Phys. Lett.* **B 399** (1997) 329
18. ALEPH Col., *Eur. Phys. J.*, **C 12** (2000) 183
19. DELPHI Col., CERN-EP-99-005
20. DELPHI Col., *Phys. Lett.* **B 456** (1999) 310
21. L3 Col., *Phys. Lett.* **B 370** (1996) 195
22. L3 Col., *Phys. Lett.* **B 407** (1997) 361
23. L3 Col., *Phys. Lett.* **B 433** (1998) 163
24. OPAL Col., *Phys. Lett.* **B 391** (1997) 221
25. OPAL Col., *Eur. Phys. J.*, **C 2** (1998) 441
26. OPAL Col., *Eur. Phys. J.*, **C 6** (1991) 1
27. OPAL Col., *Eur. Phys. J.*, **C 13** (2000) 1
28. M.-N. Minard, "Fermion pair production at LEP-2 from 130 to 196 GeV", in EPS-HEP-99, cf. ref. [1].
29. Barbiellini et al., *Phys. Lett.* **B 106** (1981) 414
30. K.J.F.Gaemers et al., *Phys. Rev.* **D 19** (1979) 1605
31. C. Caso et al.,"The 1998 Review of Particle Physics",*Eur. Phys. J.*, **C 3** (1998) 1
32. L3 Col., *Phys. Lett.* **B 470** (1999) 268
33. ALEPH Col., *Phys. Lett.* **B 401** (1997) 347
34. ALEPH Col., *Phys. Lett.* **B 415** (1997) 435

35. ALEPH Col., *Phys. Lett.* **B 453** (1999) 107
36. DELPHI Col., *Phys. Lett.* **B 397** (1997) 158
37. DELPHI Col., *Eur. Phys. J.*, **C 2** (1998) 581
38. L3 Col., *Phys. Lett.* **B 398** (1997) 223
39. L3 Col., *Phys. Lett.* **B 407** (1997) 419
40. L3 Col., *Phys. Lett.* **B 436** (1998) 437
41. OPAL Col., *Eur. Phys. J.*, **C 1** (1998) 395
42. OPAL Col., *Eur. Phys. J.*, **C 8** (1999)) 191
43. A.J. Barczyk, "W Boson Properties at LEP", talk at EPS-HEP-99 Conference, cf. ref. [1].
44. J. Ellison, "W and Z Properties at the Tevatron", talk at EPS-HEP-99 Conference, cf. ref. [1].
45. ALEPH Col., *Phys. Lett.* **B 422** (1998) 369
46. ALEPH Col., *Phys. Lett.* **B 445** (1998) 239
47. DELPHI Col., *Phys. Lett.* **B 317** (1997) 158
48. DELPHI Col., *Phys. Lett.* **B 423** (1998) 194
49. DELPHI Col., *Phys. Lett.* **B 459** (1999) 382
50. L3 Col., *Phys. Lett.* **B 398** (1997) 223
51. L3 Col., *Phys. Lett.* **B 413** (1997) 176
52. L3 Col., *Phys. Lett.* **B 467** (1999) 171
53. OPAL Col., *Phys. Lett.* **B 397** (1997) 147
54. OPAL Col., *Eur. Phys. J.*, **C 2** (1998) 597
55. OPAL Col., *Eur. Phys. J.*, **C 8** (1999) 111
56. O. Yushenko, "Single W production and neutral TGC at LEP-2", talk at EPS-HEP-99, cf. ref. [1].
57. ALEPH Col., *Phys. Lett.* **B 401** (1997) 347
58. ALEPH Col., *Phys. Lett.* **B 422** (1998) 384
59. ALEPH Col., *Phys. Lett.* **B 453** (1999) 121
60. DELPHI Col., *Phys. Lett.* **B 397** (1997) 158
61. DELPHI Col., *Eur. Phys. J.*, **C 2** (1998) 581
62. L3 Col., *Phys. Lett.* **B 398** (1997) 223
63. L3 Col., *Phys. Lett.* **B 413** (1997) 176
64. L3 Col., *Phys. Lett.* **B 454** (1999) 386
65. OPAL Col., *Phys. Lett.* **B 389** (1996) 416
66. OPAL Col., *Eur. Phys. J.*, **C 1** (1998) 395
67. OPAL Col., *Phys. Lett.* **B 453** (1999) 138
68. T. Muta, R. Najima ans S. Wakaizumi, Mod. Phys. Lett. A1 (1986) 203
69. A. Juste, "Measurement of the W mass in e^+e^- annihilation", Thesis, Univ. Autonoma de Barcelona, 1998 (unpublished).
70. Ll. Mir, "W mass from hadronic decays at LEP", talk at EPS-HEP-99, cf. ref. 1.
71. I. Riu, "Measurement of the W mass from the $WW \to qqqq$ channel with the ALEPH Detector", Thesis, Univ. Autonoma de Barcelona, 1998 (unpublished).
72. E. Torrence, "Determination of the LEP Beam Energy", talk at EPS-HEP-99, cf. ref. 1.
73. B. Carithers, "New W mass results from CDF and D0", talk at EPS-HEP-99, cf. ref. 1.
74. G. Quast, "Z parameters and Electroweak Fits", talk at EPS-HEP-99, cf. ref. 1.
75. M. Spira and P. Zerwas, "Electroweak Symmetry Breaking and Higgs Physics" CERT-TH/97-379,DESY 97-261,hep-ph/9803257.
76. J. Ellis, "Phenomenology of LEP2 Physics", Lecture at Lake Louise Winter Institute, Feb. 1977, CERN-TH/97-131.
77. F. Richard, "Search for Higgs Bosons in e^+e^- Colliders". Preprint LAL 98-74.
78. ALEPH Col., *Phys. Lett.* **B 412** (1997) 155
79. ALEPH Col., *Phys. Lett.* **B 440** (1998) 403
80. ALEPH Col., *Phys. Lett.* **B 447** (1998) 336
81. DELPHI Col., *Eur. Phys. J.*, **C 2** (1998) 1
82. DELPHI Col., *Eur. Phys. J.*, **C 10** (1999) 563
83. L3 Col., *Phys. Lett.* **B 411** (1997) 373
84. L3 Col., *Phys. Lett.* **B 431** (1998) 437

85. L3 Col., *Phys. Lett.* **B 461** (1999) 376

86. OPAL Col., *Phys. Lett.* **B 393** (1997) 231

87. OPAL Col., *Eur. Phys. J.*, **C 1** (1998) 425

88. OPAL Col., *Eur. Phys. J.*, **C 7** (1999) 407

89. A. Read, "Searches for the SM Higgs Boson at LEP with $\sqrt{s} \leq 189GeV$", talk at EPS-HEP-99, cf. ref. 1.

90. E. Gross, "Searches for New Particles", talk at EPS-HEP-99, cf. ref. 1.

91. E. Gross, A. L. Read and D. Lellouch, "Prospects for the Higgs Boson Search in e^+e^- Collisions at LEP 200", CERN-EP/98-094.

92. LEP working group for Higgs searches, CERN-EP/99-060.